Antifriction aminopropyltriethoxysilane films on thermoplastic elastomer substrates using an APPJ system

Elisa Sainz-García[1], Fernando Alba-Elías[1*], Rodolfo Múgica-Vidal[1], Ana González-Marcos[1]

[1] Department of Mechanical Engineering. University of La Rioja. c/ Luis de Ulloa 20, 26004 Logroño, La Rioja, Spain.

Accepted Version for publication in Surface and Coatings Technology

Link to publisher version (DOI): https://doi.org/10.1016/j.surfcoat.2016.12.079

Published source citation:

Sainz-García, E., Alba-Elías, F., Múgica-Vidal, R., & González-Marcos, A. (2017). Antifriction aminopropyltriethoxysilane films on thermoplastic elastomer substrates using an APPJ system. Surface and Coatings Technology, 310, 239-250. https://doi.org/10.1016/J.SURFCOAT.2016.12.079

Title: Antifriction aminopropyltriethoxysilane films on thermoplastic elastomer substrates using an APPJ system

Author names and affiliations:

Elisa Sainz-García
Department of Mechanical Engineering
University of La Rioja
c/ Luis de Ulloa 20, 26004 - Logroño, La Rioja, Spain.
Tel.: +34 941299276; fax: +34 941299794.
E-mail address: elisa.sainzg@unirioja.es

Rodolfo Múgica-Vidal
Department of Mechanical Engineering
University of La Rioja
c/ Luis de Ulloa 20, 26004 - Logroño, La Rioja, Spain.
Tel.: +34 941299276; fax: +34 941299794.
E-mail address: rodolfo.mugica@alum.unirioja.es

Dr. Ana González-Marcos
Department of Mechanical Engineering
University of La Rioja
c/ Luis de Ulloa 20, 26004 - Logroño, La Rioja, Spain.
Tel.: +34 941299276; fax: +34 941299794.
E-mail address: ana.gonzalez@unirioja.es

Corresponding author:
Dr. Fernando Alba-Elías
Department of Mechanical Engineering
University of La Rioja
c/ Luis de Ulloa, 20, 26004 - Logroño, La Rioja, Spain.
Tel.: +34 941299276; fax: +34 941299794.
E-mail address: fernando.alba@unirioja.es

ABSTRACT

The study of friction coefficients has long been of great importance in the automotive industry where some areas of the vehicle are subject to slippage. One example is the space between the window channels and the glass. The polymeric materials that are used in these areas, like thermoplastic elastomers (TPE), involve a high degree of friction. So, in order to decrease the friction coefficient of the TPE, companies are using such techniques as flocking. However their high energy consumption, irregular distribution of fibers and poor adhesion are drawbacks. In order to overcome these drawbacks, this work attempts to obtain a SiOx-based thin film over a TPE substrate using aminopropyltriethoxysilane (APTES) with similar or lower friction coefficients and the same durability. Since TPE is heat-sensitive, an atmospheric-pressure plasma jet system (APPJ) with a dielectric barrier discharge (DBD) was used in this study. The influence of the plasma power and number of passes was characterized by Profilometry, Atomic Force Microscopy (AFM), Scanning Electron Microscopy (SEM), Attenuated Total Reflectance-Fourier Transform Infrared (ATR-FTIR) Spectroscopy, X-Ray Photoelectron Spectroscopy (XPS), Water Contact Angle (WCA) measurements and friction coefficient. The average surface temperature of the samples and the coating thickness seem to be the key variables in determining the friction behavior. Successful samples (those that have a lower friction coefficient than those of the current industrial solutions - flocked seals and polyamide tap) were coated at an average surface temperature of less than 92 ºC and thicknesses of the coatings were greater than 1000 nm. Sample coated in six passes and the lowest power (350 W) proved to have the best friction performance. This sample has a friction coefficient that is 46% lower than that of the flocked seals. The results of this research permit one to conclude that a promising

antifriction technology using APPJ with a DBD could be an alternative to the current industrial solutions.

1 Introduction

The study of friction coefficients and wear mechanisms has long been of great importance in the operation of many mechanical systems. In fact, many industrial applications require low friction coefficients. In the automotive industry, some areas of the vehicles are subjected to slippage. These include the space between the window channels and the glass, and between the wind-shield and the wind-shield wipers, where a low friction coefficient is necessary to prevent jams. Furthermore, a high hydrophobicity would be desirable in order to evacuate the stored water in the operation. The polymeric materials that are used in these areas, like thermoplastic elastomers (TPEs), intrinsically involve high friction [1]. So, in order to improve friction performance, companies are using two different techniques, such as flocked seals and a polyamide tape affixed to the tape seals. Today, the flocked method is widely used in the automotive sealing industry due to its low friction coefficient. The high energy consumption and long installation lines, together with an irregular distribution of fibers, poor fiber orientation and poor adhesive distribution are the main drawbacks of this technology [2].

Plasma technology is becoming more and more popular as a means to modify the intrinsic properties of substrate materials by coating or activation [3–5]. Operating at atmospheric pressure in a dielectric barrier discharge configuration is particularly suitable for the treatment of temperature-sensitive materials, such as polymers, since it generates cold plasmas [5,6].

The friction and wear of a material depend primarily on its surface properties [7]. Previous studies of plasma-polymerized siloxane coatings, like hexamethyldisiloxane

(HMDSO) or aminopropyltriethoxysilane (APTES), have demonstrated a reduction in the friction coefficient on different substrates [8–10].

This paper deals with the synthesis and characterization of SiOx-based coatings that are deposited on TPE substrates that have been produced by an Atmospheric Pressure Plasma Jet (APPJ) system. The main purpose is to obtain a coating that has friction coefficients that are similar to, or lower than, the current industrial solutions (flocked seals and polyamide tape) with the same or greater durability. It would be desirable also to obtain a wettability behavior that is similar to or better than those of these industrial solutions. In addition, this coating method would reduce considerably the manufacturing cost, which is one of the most important concerns when developing a viable coating for an industrial application [11].

The influence of the different process parameters, mainly plasma power and deposition time (number of passes), in depositing coatings on TPE was characterized from morphological, chemical and mechanical points of view by Profilometry, Atomic Force Microscopy (AFM), Scanning Electron Microscopy (SEM), Attenuated Total Reflectance-Fourier Transform Infrared (ATR-FTIR) spectroscopy, X-Ray Photoelectron Spectroscopy (XPS), Water Contact Angle (WCA) measurements and friction coefficient.

2 Experimental Details

2.1 Materials and sample deposition

SiO_2-based coatings of various thicknesses were deposited on flat TPE substrates of 100 mm x 50 mm x 2 mm that were vulcanized from pellets of Santorene^{TM} 121-67W175 (ISO 18064).

A schematic diagram of the atmospheric pressure plasma jet (APPJ) system of PlasmaSpot® that was used to coat the samples is shown in [1]. This system consists of an Al_2O_3 dielectric tube between two cylindrical electrodes; the outer electrode is connected to high voltage during operation and the inner electrode is grounded.

The jet moved across the sample´s surface at a scanning speed of 6 m/min and a track pitch of 2 mm. The gap between the discharge plasma and the substrate was set at 6 mm. Nitrogen was used as the plasma gas at 80 slm. The chemical precursor, 3-aminopropyltriethoxysilane (APTES), was purchased from Sigma Aldrich and used as received. A fine aerosol of liquid APTES was created using an atomizer. The inlet gas for the atomization was nitrogen at 1.5 slm and the size of the generated droplets ranged from 10 nm to 300 nm. With the aim of preventing a direct contact of APTES fumes with the plasma operator, due to its toxicity, the coating process was implemented using a fume hood. The ozone generated from the air during the atmospheric pressure process is evacuated with the same system. The APTES fume from the atomizer is directly transported to the inner electrode via a silicone tube. At the bottom of the inner electrode, the APTES fume contacts with the plasma.

Twelve different samples were coated as **Table 1** shows. For each sample the coating process consisted of two steps, in which the same plasma power at a frequency of 68 kHz was used. In the first step, the sample was scanned once to activate the surface. During this activation step, no precursor was introduced into the jet. Only nitrogen was used as plasma gas. With the aim of studying the effect of the activation step, three activated samples with different plasma power (A1/350, A1/450 and A1/550) were analyzed (see **Table 1**). After activation, a process of plasma-polymerization with APTES was carried out. Depending on the sample, the jet was moved across the substrate surface as many times as **Table 1** indicates (number of passes).

In order to evaluate the effect of surface temperature on the properties of the coated samples, the temperature was measured continuously during the coating process using a temperature sensor that was taped to the sample´s surface for the 18-pass samples (S18/350, S18/450 and S18/550).

2.2 Sample characterization techniques

The thickness of the coatings has been evaluated by surface profilometry using a Taylor Hobson Surtronic 25 profilometer, which provides data analysis and images captured by scanning. The scanning length that was chosen was 4 mm and the range was 100 μm. Before coating the samples, the TPE´s surface was partially covered by a mask. After the coating process, the mask was removed and the step´s height was measured by the mechanical profilometer. The average coating thickness of five measurements from each sample was determined.

An XE-70 Atomic Force Microscopy system (AFM) (Park systems) was used to explore the surface topography and the roughness of the samples. Areas of 40 μm x 40 μm were scanned in non-contact mode with a silicon cantilever (Nanosensors^{TM} PPP-NCHR). Data processing was done by applying a plane fit algorithm. The root mean square (RMS) roughness was calculated as the average value of the measurements of three different spots per sample by means of NanoScope Analysis 1.4 software.

The surface morphology of all the samples was examined by use of a Scanning Electron Microscope (SEM) HITACHI S-2400 at an operating voltage of 18 kV. Samples that were analyzed were made conductive by gold-palladium sputtering before introduction to the SEM chamber to prevent charging during SEM analysis. An energy dispersive X-ray spectroscopy (EDX) that was installed in the SEM was used to study the atomic chemical composition of the uppermost layer of the coatings and the wear tracks.

Attenuated Total Reflectance-Fourier Transform Infrared (ATR- FTIR) spectroscopy spectra were recorded on a Bruker Tensor 27 spectrometer that was equipped with a single reflection ATR accessory for chemical bond characterization of the samples. For each spectrum, 32 scans were collected and averaged in the range of 600-4000 cm^{-1} at a 4 cm^{-1} resolution.

The atomic chemical surface composition of the samples was monitored using a Physical Electronics PHI 5700 spectrometer with a multi-channel hemispherical analyzer, a pass energy of 29.35 eV and MgKα (1253.6 eV) X-radiation (XPS). XPS deconvolutions were undertaken with the PeakFit 4.12 (SPSS Inc.) software by fitting each spectrum with a mixture of Gaussian-Lorentzian functions. A 285 eV binding energy related to the C1s signal was used to calibrate the energy scale for XPS deconvolutions.

To determine the wettability of the samples, the static water contact angles (WCA) were measured by the sessile drop method. The WCA value of each sample was calculated as an average of four measurements (10μL/drop) by image analysis.

In order to study the tribological performance of the analyzed samples, tribological tests were conducted with a CSM tribometer using the ball-on-disk method. This method consists of a 100 Cr6 steel ball (60-62 HRC, 6 mm in diameter) that is in contact with the surface of the sample with an applied load. The sample is spun and the steel ball makes a circular groove in the sample. The test parameters that were established were a sliding speed of 2 cm/s, a radius of 2.5 mm, a normal load of 1N and a test length of 4000 m.

2.3 Surface temperature of the coatings

Fig. 1 shows the average surface temperature as a function of the number of passes. During the deposition process, the ambient air temperature was maintained constantly at 21ºC. The sample holder was not equipped with a heating or cooling instrument. **Fig. 1** shows clearly that the average surface temperature rises slowly with the number of passes for a given power (350, 450 or 550 W). This increase is due to the energy stored in the plasma and the coating during the deposition process [12]. The longer the deposition process is, the higher is the surface temperature that is reached. For a selected number of passes, an increase in the average temperature is observed when the power of the plasma polymerization process is raised. That is, the surface temperature is strongly dependent on the power [13]. A higher power results in more energetic ions, molecules and particulates [14–16], which may cause plasma etching of the coating surface. As some studies have discovered [17–20], the surface temperature of the samples and its residence time can have a great impact on chemical composition and structure, surface morphology and mechanical performance of the as-deposited samples, especially when temperature-sensitive substrates, such as TPE, are used [21]. This is the reason why the following sections contain a detailed study of morphology, chemical composition and friction behavior.

3 Results and Discussion

3.1 Coating thickness

3.1.1 Effect of the number of passes

Fig. 2 [a] and **Table 2** show the thickness and standard deviation of the deposited coatings. **Fig. 2 [a**] shows that, for a specific power, the coating thickness increases in linear fashion with the number of passes. That is, the thickness of the coating is a function of the deposition time. The reason is that the plasma jet is working longer,

since it passes over the sample's surface more times. This causes further growth of the coatings with a consequent increase in thickness.

The growth rate of each sample was obtained by dividing its film thickness by the number of passes. As shown in **Fig. 2[b]**, it was discovered that the curve of the growth rate for a specified power reaches a maximum at about six passes followed by a linear decrement for up to eighteen passes [22,23]. This behavior seems to be related to the roughness of the samples, since the curve of the roughness (**Fig. 3**) shows an inverse shape to that of growth rate. In this respect, when the 2-pass samples are coated, the surface exposed to plasma-polymerization appears to be largely determined by the roughness of the uncoated TPE sample. During this process, the cavities of the uncoated TPE are being filled and as the number of passes increases (from 2 to 6 passes), the sample becomes increasingly smooth. This decrease in roughness causes the area exposed to plasma-polymerization to be lower, resulting in a higher growth rate. When reaching 6 passes, the roughness values for these samples are the lowest and therefore the area exposed to the plasma-polymerization are the lowest. Given that the precursor flow rate is constant (1.5 slm) throughout the deposition process, a decrease of the area exposed to the plasma-polymerization involves an increase of the growth rate. As the number of passes increases (from 6 to 18 passes), the roughness increases due to the growth of the particles. This causes an increase of the area exposed to the plasma-polymerization which in turn results in a decrease in growth rate.

3.1.2 Effect of the plasma power

In **Fig. 2**, neither the thickness nor the growth rate of the coatings changed significantly with plasma power. In **Table 2**, one can see the high standard deviations (SD), which exceed 25 percent of the coating´s thickness in many cases. This is explained by the

growing mechanisms and the morphology of the coatings over the TPE substrate, as is mentioned below.

3.2 Surface morphology

3.2.1 Effect of the number of passes

Fig. 3 depicts the average roughness of all the samples. In this figure, one can see that, for a given power, the roughness increases as the number of passes increases.

It is noteworthy that, for a specified power, the roughness of samples that were coated in two passes (S2/350, S2/450 and S2/550) is slighly higher than the roughness of samples that were coated in six passes (S6/350, S6/450 and S6/550). However, the surface of 2-pass samples probably has not been completely coated, since such coatings are very thin (S2/350: 230 nm, S2/450: 190 nm and S2/550: 160 nm) in comparison to TPE´s roughness (RMS: 364 nm) and its own roughness (S2/350: 401 nm, S2/450: 276 nm and S2/550: 376 nm). The reliability of the thickness measurements for 2-pass samples is questionable since it was difficult to identify if the profilometry measurements correspond to the thickness of the coating or to a discontinuity of the raw substrate. Nevertheless, the use of six passes to coat samples is sufficient to fully cover the TPE´s surface. This provides smoother coatings (S6/350: 338 nm, S6/450: 257 nm and S6/550: 322 nm) with thicknesses greater than 1000 nm (S6/350: 1524 nm, S6/450: 1483 nm and S6/550: 1402 nm).

Fig. 4 illustrates tilted SEM images, whereas **Fig. 5** shows AFM images of samples S2/350, S6/350, S6/550, S18/350, S18/550 and the uncoated TPE. **Fig. 6** shows SEM images with cracks of samples coated with 350 W and 550 W. SEM and AFM images of the uncoated TPE substrate (**Fig. 4[d] and Fig. 5[d]**) exhibit a highly fibrous aspect and some carbon particles of TPE substrate. Samples that are coated at 350 W (see **Fig.**

4[b-c] and **Fig. 5[b-c]**) exhibit a coating that consists of spherical particles that have been deposited on the TPE fibers. It would appear that the morphology of APTES coatings relies heavily on the uncoated TPE´s morphology.

In fact, it is believed that both the fibers and carbon particles of TPE substrate probably act as nucleation sites where the coating grows [24]. This agrees with the SEM and AFM images of sample S6/350 (see **Fig. 4[b]**, **Fig. 5[b]** and **Fig. 6[a]**) that show some spherical particles that have been deposited on both nucleation sites. An increase in the number of passes results in gas species remaining longer in the plasma jet. This favors precursor fragmentation and recombination of different particles during the plasma-polymerization process [25]. In turn, this causes an increase in size and number of spherical particulates as **Fig. 4[c]**, **Fig.5[c]** and **Fig. 6[c]** illustrate. Such spherical growth is also promoted by the so-called shadowing effect, which is caused by geometric interaction between the surface roughness of the growing film and the angular direction of the arriving coating species. That is, the deposition rate at the top of spherical particles is higher than at the bottom of the voids where the incident angle for arriving coating species is thinner. [22,24]. As a result of this growth mechanism, there is an increase in roughness (S6/350: 338 nm → S18/350: 724 nm) and thickness of the coatings (S6/350:1524 nm → S18/350: 2938 nm).

Cracking has been observed clearly on the surface of these samples under SEM analysis (as **Fig. 6**). The residual thermal stress that is due to differences between the thermomechanical properties of the coating and the TPE substrate [21,26,27], and the coating embrittlement by the higher number of passes may be two of the main causes of cracking [4]. It should be noted that the size of the cracks is the greatest in the samples that were coated in the greatest number of passes. This can be related to the

cumulative effect of the surface temperature due to the longer exposure of the sample to an energetic plasma, as can be seen in **Fig. 1** [28,29].

3.2.2 Effect of the plasma power

Fig. 7 illustrates SEM images of the uncoated TPE together with the samples activated with 350 W and 550 W. In these images, one can observe that the activation process cause a slight etching of the substrate. Moreover, the roughness of the activated samples are slightly higher than the roughness of the uncoated TPE (see **Table 2**).

Related to the coated samples, the higher the plasma power (350 W→550 W) is, the greater is the precursor decomposition during the gas phase reactions of the plasma and the higher is the number of small particulates on the coating surface [1]. In fact, one can compare the size and number of particulates of samples that have been coated in six passes (**Fig. 4[b]-[e]**, **Fig. 5[b]-[e]** and **Fig. 6[a]-[d]**), and note a higher number of smaller particles on samples that have been coated at higher plasma power.

The same applies to 18-pass samples (**Fig. 4[c]-[f]**, **Fig. 5[c]-[f]** and **Fig. 6[c]-[f]**), which result in a decrease in roughness with increasing power (S18/350: 724 nm and S18/550: 629 nm), since spherical particles create a denser and more compact coating that fits the uncoated TPE´s morphology better [18,30]. The more energetic ions, molecules and particles that are achieved with higher plasma powers cause an increase in the average surface temperature of the samples (see **Fig. 1**).

The ions that bombard the sample surface are needed to ensure smooth and dense coatings. However, in certain cases, they may become too powerful and cause an increase in the temperature of the sample. This increase, if followed by cooling of the sample after the coating process, generates residual thermal stress. The impact of residual thermal stress will be discussed in Section *3.5 Tribological tests*.

Fig. 8 shows the AFM profiles of sample S6/350 and samples that were coated in eighteen passes (S18/350, S18/450 and S18/550). All of the studied profiles were obtained following the TPE´s fibers direction that, it is believed, act as nucleation sites. By comparing samples that were coated with the same power (S6/350 and S18/350) (**Fig. 8[a] and [b)**], one can confirm the aforementioned increase in both the diameter and the number of particles with a higher number of passes.

In regard to the samples that were coated with the same number of passes and different powers (**Fig. 8[b-d]**), the profile of sample S18/350 evinces a small number of spherical particles with large diameters (~5 μm). The greater the power is, the smaller is the diameter, and the higher is the number of particles. In this way, sample S18/450 exhibits an average diameter of ~3 μm and sample S18/550 shows an average diameter of ~1.5 μm with many particles.

Regarding the crack formation, one can observe in **Fig. 6** that the higher the power is, the greatest the number of cracks is. This is probably due to the temperature effect, which is similar to what happens with the increment of the number of passes.

Considering the aforementioned, one can conclude that the SEM results are in good agreement with the AFM images and confirm that the surface roughness was affected significantly by the deposition conditions. In this regard, **Fig. 9** illustrates a scheme of the growth mechanisms of coating by the plasma power and number of passes. In **Fig. 9**, one can see the strong influence of the substrate´s morphology during the early growth stages. As the number of passes increases, the fibrous aspect of the substrate is replaced progressively by a coating that consists of spherical particles from the gas phase reactions. The number and size of the particles depend on the plasma power. Once cavities and holes in the TPE substrate have been covered fully (samples S6/350 and S6/550), the coating´s morphology depends, essentially, on the number and size of

the spherical particles that have been generated and deposited. This explains the morphology of samples that have been coated in eighteen passes.

3.3 ATR-FTIR analysis

ATR-FTIR spectroscopy was used to examine the chemical characteristics of all the analyzed samples. **Fig. 10** shows the spectra of the uncoated TPE together and the activated samples (A1/350, A1/450 and A1/550). **Fig. 11** and **Fig. 12** depict the ATR-FTIR spectra of samples that were coated at 350 W (S6/350, S12/350 and S18/350) and in six passes (S6/350, S6/450 and S6/550) respectively in the 0-4000 cm^{-1} range. Chemical bonds that are shown in these figures correspond only to the chemical composition of the coatings. Chemical bonds that correspond to the uncoated TPE substrate are not shown in these figures since the thickness of these coatings exceeds the depth of analysis of this technique (<1000 nm). **Fig. 13** shows the ATR-FTIR spectrum of the uncoated TPE sample and samples S2/350 and S2/550. Considering that the thickness of 2-pass samples is less than 1000 nm (see **Table 2**), the contribution of the uncoated TPE signal was subtracted from their absorption spectrums.

The main peaks of the uncoated TPE spectrum were described in an earlier work by these authors [10]. As shown in **Fig. 10**, the same peaks that are observed in the characteristic spectrum of the uncoated TPE are also identified in the activated samples. However, the activated samples exhibit a new wide band that is located in the range ~1600-1700 cm^{-1} corresponding to C=O and C=C bonds [31]. The spectra of the coated samples contain peaks at ~720 and ~805 cm^{-1} that are related to -CH_2 rocking and Si-C/SiOSi bending vibration functional groups, respectively [14,29,30]. In the range 840-1250 cm^{-1}, a broad band can be seen that corresponds to six different overlapping functional groups: methyl rocking mode at ~950 cm^{-1} [4], a stretching vibration of

SiOSi at ~1050 cm^{-1} [10], the SiOC ring link at ~1074 cm^{-1} [10], the SiOC open link at ~1115 cm^{-1} [10,32], the SiOC cage link at ~1172 cm^{-1} [10,32], and OCH_2CH_3 at ~1200 cm^{-1} [10,33]. Different peaks can be identified in the range of ~1250-1500 cm^{-1}, which account for the stretching mode of Si-$(CH_3)_x$, C-N, C=O, and C-C groups [14,29,34]. The band in the region of ~1500-1700 cm^{-1} is attributed to amine and amide functional groups [10,34]. The band in the region ~2800-2950 cm^{-1} is related to CH_x stretching modes [4,34]. Finally, the broad band in the 3000-3600 cm^{-1} range can be attributed to various functional groups: -OH from SiOH and/or absorbed H_2O and NH_X stretching [17,18,29].

3.3.1 Effect of the number of passes

It is evident in a comparison of the peak intensity of the spectrum of the samples that were coated at 350 W, as **Fig. 11** shows, that the lower the number of passes is, the higher the ATR-FTIR spectrum intensity is. This trend is probably explained by the coating morphology. In Section *3.2 Surface morphology*, it was seen that a higher number of passes resulted in an increase in the number and size of spherical particles of the coating (see **Fig. 4** and **Fig. 5**) leading to a greater roughness. So, as **Fig. 8[a] and [b]** illustrate, sample S18/350 (RMS: 724 nm) exhibits a voided profile with higher roughness than sample S6/350 (RMS: 338 nm). Bearing in mind that the analysis depth of the ATR-FTIR technique is less than 1000 nm together with the thickness of these two samples (greater than 1000 nm), the intensity signal of the functional groups of sample S18/350 would be penalized due to the existence of an air gap between the diamond ATR element and the sample surface. This results in a spectrum with lower intensities that is not representative of the nature of this coating [35–38].

3.3.2 Effect of the plasma power

For the activated samples, the higher is the plasma power, the lower is the absorbance areas of peaks located at ~1100 (C-O) and ~2800-2950 (CH_x) cm^{-1} and the higher is the absorbance areas of the bands in the range ~1600-1700 (C=O and C=C) and ~3000-3600 (OH) cm^{-1} (see **Fig. 10**). It seems that an increase in plasma power causes the breakage of low energy bonds (C-O: ~351 and CH_x: ~413 kJ/mol) and the formation of stronger bonds (C=O: ~745, C=C: ~612 and OH: ~460 kJ/mol).

Samples that have been coated in six passes have a similar thicknesses and roughnesses (S6/350: 1524 nm/338 nm; S6/450: 1483 nm/257 nm; S6/550: 1402 nm/322 nm). This is the reason why the FTIR spectra of these samples show similar peaks and intensities (**Fig. 12**), with a slight difference in the intensity of the broad band that is found around 1050 cm^{-1}. However, although some authors have identified a relationship between the area under the SiOSi peak (~1050 cm^{-1}) and the tribological properties of the coatings [1,10,39], there is no relationship to the 6-pass samples. This is probably due to the harmful effect of the temperature that is reached during the coating process. This effect will be discussed in Section *3.5 Tribological tests*.

It appears that temperature does not affect the samples that were coated in less than six passes, since both the average surface temperature of the samples and their residence times have not been sufficiently high to compromise the quality of the coatings. In fact, ATR-FTIR of 2-pass samples in **Fig. 13** show an increase of the area under the SiOSi peak at the power that is related to lower friction coefficients, as will be detailed in Section *3.5 Tribological tests.*

3.4 XPS analysis

In regard to the chemical composition, XPS analysis, with an analysis depth of 10 nm [40,41], was used to quantify the atomic composition of the uncoated TPE, activated

and coated samples. **Table 3** shows the atomic chemical composition of these samples. Deconvolutions of the Si2p signal of the samples that were coated at 350 and 550 W were undertaken (**Table 4**) to develop a better quantification of the relative percentages of SiO_2, SiO_3 and SiO_4 and its relation to the tribological behavior. **Fig. 14** shows the atomic percentages of C1s, O1s, Si2p and N1s of samples that were coated at 350 W (S6/350, S12/350 and S18/350) and in eighteen passes (S18/350, S18/450 and S18/550), respectively.

Related to the activated samples, the chemical composition of the sample activated at 550 W (A1/550) and the uncoated TPE are very similar. The same applies to samples activated with 350 W and 450 W. It appears that the surface of samples activated with lower power experiences higher oxidation.

In **Table 3** and **Fig. 14**, one can see that, for coated samples, the C1s percentage varies between 51.4% and 60.0%, the O1s percentage varies between 23.3% and 28.7%, the Si2p percentage varies between 11.8% and 16.6% and the N1s percentage between 3.3% and 4.2%. These variations do not allow to justify the tribological behavior as it will be discussed in section *"3.6 Tribological tests"*.

However, one can see in **Table 3** the increase in the atomic percentage of Si2p and O1s and the subsequent decrement of C1s percentage of coated samples with respect to the atomic percentages of the uncoated TPE sample. In addition, ATR-FTIR and XPS results of the coated samples showed that the major bond of SiOx based-films is SiOSi with characteristics peaks at 805 cm^{-1} and ~1050 cm^{-1}, and the O/Si ratio of the films between 1.7-2.0. The latter is a value that is close to the stoichiometric ratio of silica (O/Si = 2).

In regard to the Si2p deconvolutions (see **Table 4**), it is noted that, for a selected number of passes, the SiO_4 percentage increases with the plasma power, indicating a more inorganic character of the coatings.

3.5 Wettability

To investigate the wettability of the samples, water contact angles (WCA) of all samples were measured. It is known that the wettability of a surface is affected by the chemical composition of the first 3 nm surface layer and the surface roughness of the coatings [14,41]. **Fig. 15** illustrates the WCA of the coated samples, uncoated TPE and the polyamide tape. It was not possible to determine the WCA of the flocked seals, since it consisted of polyethylene fibers.

On one hand, the WCA of the activated samples (A1/350: 88.4º ± 3.9, A1/450: 89.8º ± 3.1 and A1/550: 93.5º ± 1.2) were slightly higher than the uncoated TPE one (86.0º ± 6.4) probably due to the higher roughness of these samples after the activation step. On the other hand, for the coated samples, changes in WCA seem to be explained by its differences in roughness together with the inorganic character of the coatings. It was discovered in Section *3.2 Surface morphology* that the growth mechanisms and the roughness of the coatings depend on the number of passes and the plasma power. In addition to this, the inorganic character of the coatings depends on the SiO_4 (**Table 4**). All coated samples, with the exception of sample S6/550, have a WCA that exceeds that of the polyamide tape (85.1º ± 7.4) and the uncoated TPE (86.0º ± 6.4).

3.5.1 Effect of the number of passes

For any power, as shown in **Fig. 15**, WCA usually increases with an increase in the number of passes from 2 to 18. These results can often be explained by the roughness values (see **Fig. 3**). Increasing the number of passes from 6 to 18 for a given power

increases the roughness and, therefore, the WCA. Similarly, increasing the number of passes from 2 to 6 decreases the roughness and, therefore, the WCA (except for 350W). The wetting behavior of the coatings can be ascribed to the formation of spherical particles that create a roughness. The higher the number of passes is, the greater is the size and the number of particles.

In turn, this leads to greater roughness. Therefore, it can be concluded that a rise in WCA is caused by an increase in roughness as other studies have demonstrated [14].

3.5.2 Effect of the plasma power

Despite the high standard deviation (SD) of WCA (see **Fig. 15**), it seems that an increase in plasma power from 350 to 550 W results in a lower WCA, for samples that have been coated in 6, 12 or 18 passes. This is in agreement with the increasing inorganic character of the samples with higher power as one can see in **Table 4**.

In previous works of this research group, WCAs were related to the roughness of the coatings [2]. However, in this work, although a decrease of the roughness with the power could be observed in **Fig. 3**, the variations are not so significant as to ensure that such relation is complied.

WCAs of samples that have been coated in two passes are practically the same (~87º) and are very similar to the uncoated TPE WCA (86.0º ± 6.4). It seems that the use of two passes generates an incomplete coverage of the substrate. Thus, there is a minimum number of passes necessary for full-coverage the substrate surface [42].

For samples whose roughness is similar to that of uncoated TPE (RMS: 364±32 nm), differences in WCAs are explained by their chemical composition, since after deposition of an APTES-based coating, the wettability of the sample increased in agreement with the presence of SiOx groups that are characteristics of the APTES molecule. As an example, sample S6/350, whose RMS is 338 nm, has a WCA that is

considerably greater than that of the uncoated TPE (S6/350: 102.0º ± 6.6 and uncoated TPE: 86.0º ± 6.35), since the uppermost layer of this sample consists of SiOx, with an O/Si ratio of 1.9, which is close to the stoichiometric ratio of silica (O/Si = 2). Furthermore, the cracks observed in SEM images likely result from the evolution of the coating to a silica structure [4].

3.6 Tribological tests

The coefficients of friction (CoF) of samples that were coated at 350 and 550 W together with the uncoated TPE sample and the current industrial solutions (flocked seals and polyamide tape) appear in **Fig. 16**, **Fig. 17** and **Table 5** show the average friction coefficient of the coated samples and the uncoated TPE.

A friction test with a sliding distance of 4000 m was selected to reproduce the rigors of the operation that the coating on a seal of a vehicle undergoes during its lifetime. This distance is much longer than that used in previous work [1,10,30]. In the beginning of this paper, it was mentioned that one of the main goals was to obtain coatings that could replace the solutions that are used in automotive sealing today (flocked seals and polyamide tape), especially to eliminate the slippage between the window channels and the glass. Therefore, a coating with lower friction coefficient and the same or greater durability than these technical solutions is necessary. The average friction coefficient of a flocked seal is 0.25 ± 0.06, whereas that of a polyamide tape is 0.28 ± 0.01. The friction coefficient of the activated samples was similar to the uncoated TPE one (0.68±0.02).

Fig. 16 shows that the friction coefficient of the flocked seal gradually increases to 3000 m, reaching a steady state with a friction coefficient of ~0,3. The friction coefficient of the polyamide tape is practically constant during the 4000 m of sliding distance. Finally,

it is noted that the friction coefficient of all of the coated samples is lower than that of the uncoated TPE. As previously stated, when temperature-sensitive substrates are used, both the surface temperature of the samples and its residence time have a significant influence on the tribological behavior of the coated samples. As has been mentioned, the higher the plasma power and number of passes are, the higher is the average surface temperature (see **Fig. 1**). Several authors have reported that, when the thermal expansion coefficients of substrate and coatings differ, residual thermal stress is generated [43–45]. The higher the process temperature (depending on plasma power and number of passes), the higher is the residual thermal stress of the coating. In addition, it is worth noting that the increase in residual thermal stress with coating depth reaches a maximum value in the bond area coating-substrate. The coatings under consideration are subjected to a thermal tensile stress, since the thermal expansion coefficient of TPE substrate is higher than that of the coatings. As confirmed [46], coatings that are subjected to high thermal tensile stress have a poorer friction behavior.

3.6.1 Effect of the number of passes

Fig. 16, **Fig. 17** and **Table 5** indicate that samples S6/350, S12/350 and S18/350 have the lowest friction coefficients of all analyzed samples, including the current industrial solutions (flock and polyamide tape). In addition, these friction coefficients decline slightly with a decrease in the number of passes (CoF S6/350 < S12/350 < S18/350). The best sample is S6/350 probably because this sample has been subjected to lower process time. This produces a lower average surface temperature (see **Fig. 1**), less residual thermal stress and a better friction performance. Otherwise, sample S2/350 has a friction coefficient that exceeds the remaining samples that were coated at 350 W and the current industrial solutions, probably because its surface is not fully coated (see **Fig.**

4 and **Fig. 5[a]**). Therefore, it seems that a minimum coating thickness is necessary to enhance a friction coefficient that is lower than those of the current industrial solutions. Samples that have been coated at 550 W have friction coefficients that exceed those of the current industrial solutions (see **Fig. 16** and **Fig. 17**). As can be seen in **Fig. 16** and **Table 5**, sample S2/550 has a friction coefficient that is nearly constant and is the lowest of the 550 W-samples. A comparison of the friction coefficient of samples S2/550 and S6/550 in **Fig. 16** shows that sample S6/550 has a lower friction coefficient than sample S2/550 during the first 2000 m of the test. This could be because the surface of this sample (S2/550) is not full-coverage. This would cause its friction coefficient to depend not only on the coating, but also on the TPE substrate. In contrast, the surface of sample S6/550 is full-coverage with a 1402 nm thickness coating. In addition, the coating of sample S6/550, although worn, has not reached a point at which it is subject to high residual thermal stress that could compromise the friction behavior, despite having been subjected to a high temperature (108.0 ºC) for a longer time (224 s). From the 2000 m of sliding distance to the end of the test, sample S2/550 had a lower friction coefficient than S6/550, probably because its surface was subjected to a high temperature (101.1 ºC) for only a short time (75 s). Thus, the anti-friction ability was not significantly affected by the residual thermal stress of this sample.

In **Fig. 16**, the friction coefficient of sample S6/550 shows three different behaviors. During the first stage (0-1000 m), the friction coefficient began at ~0.12 and increased linearly to ~0.19, since the first nanometers of the coating are not subjected to residual thermal stress that could worsen the anti-friction property. In the second stage (1000-2000 m), the friction coefficient fluctuated. This was probably due to successive cycles of the coating breaking and developing tribofilm. That is, after a sliding distance of 1000 m, the steel ball reached depths of coating at which the residual thermal stress

leads to coating detachment. During this process, an increase in the friction coefficient could be observed. Then, a tribofilm of detached material was formed that rubbed against the steel ball. This led to a decrease in the friction coefficient, since the tribofilm acts as a lubricant. When the tribofilm is completely worn, the steel ball may rub against the original coating and this cycle will repeat. Finally, in the third stage (2000–4000 m), there is a sharp increase in the friction coefficient. In this situation, the residual thermal stress is high enough to cause complete detachment of the coating so that tribofilm cannot be formed. The TPE surface is exposed to the steel and so the friction coefficient value is similar to that of the TPE.

Friction coefficients of samples S12/550 and S18/550 were similar during the entire test. Both samples were subjected to the highest temperatures for the longest time (113.1 ºC for 449 s and 116.3 ºC for 673 s respectively). This caused the highest residual thermal stress in these coatings. In **Fig. 16**, one can see two different stages during the friction test of these two samples. The first stage (0-600 m) is similar to the first stage that was identified for sample S6/550. The value of the friction coefficient started at ~0.23 and linearly increased to ~0.27. In the second stage (600-4000 m), there was a greater fluctuation of the friction coefficient due to successive cycles of the coating breaking. A development of tribofilm was observed that was comparable to that of the S6/550 sample. This behavior was maintained until the end of the test. However, if the sliding distance of the test was longer, it is estimated that a complete detachment of the coating would have occurred and the friction coefficient would have increased to a value close to that of the TPE that sample S6/550 experienced in its third stage.

In order to examine the quality of the coating at the end of the friction test, **Fig. 18** shows SEM wear track images and EDX analyses of sample S18/550 after a friction test of 4000 m.

In the EDX maps, the red color corresponds to carbon, the blue color represents the silicon and the yellow color is associated with oxygen. One can see in **Fig. 18[a] and [c]** different numbered regions of the coating. Region 1 corresponds to an undamaged coating area of spherical particles of SiO_x. The latter are similar to the particles of **Fig. 4[f]**, since this area has not been in contact with the steel ball during the friction test. In fact, its EDX map (**Fig. 18 [c]**) evinces a uniformly green coating of SiO_x that was derived from the mixture of silicon (blue) and oxygen (yellow). Region 2 depicts a transition area. This region is shown as a brittle coating where the detected cracks of Region 1 have become wider and the spherical particulates of the surface have been eroded. Region 3, together with **Fig. 18[b] and [d]**, represents the central area of the wear track, in which flattened areas of SiOx (green) of the remaining coating and tribofilm appear. The wear in this region caused the coating to detach, which resulted in areas where the TPE substrate can be observed (red color of carbon). These images show debris of the coating (white circles in **Fig. 17[c] and [d]**) from which the tribofilm is created. These flattened areas of SiOx at the end of the friction test ensure that the value of the friction coefficient is 50% less than that of the uncoated TPE.

3.6.2 Effect of plasma power

Fig. 17 and **Table 5** indicate that, for samples that were coated in 6, 12 or 18 passes, the higher the power was, the higher the friction coefficient was for a selected number of passes. This could be related to the more energetic plasma and the subsequent high temperature to which both the coating and the TPE substrate were subjected during the deposition process. These could result in an increase in the residual thermal stress of the sample after cooling to room temperature (21 ºC). As was discussed earlier, residual thermal stress has a negative impact on the friction behavior of the samples.

However, the opposite result was found with 2-pass samples. Higher power led to lower friction coefficients. These samples were subjected to different average surface temperatures for the shortest residence times (75 s). This produced lower residual thermal stress than for other samples that were coated in a higher number of passes. In such a situation, the friction behavior seems to depend on the chemical composition of the coatings as was demonstrated by other authors [1,2,10]. In this regard, the sample that was coated at 550 W (S2/550) had the highest absorption area under the SiOSi peak in the ATR-FTIR spectrum (see **Fig. 13**) and the highest SiO_4 percentage (7.0%) after the Si2p deconvolution in XPS analyses (see **Table 4**). This provided a friction coefficient that was less than those of the samples that were coated at a lower power (S2/350 and S2/450).

4 Conclusion

Plasma polymerized films of APTES over TPE substrates were prepared successfully by use of an APPJ system to obtain a higher WCA and lower friction coefficient than those of the current industrial solutions (flocked seals and polyamide tape). The key findings of this research are the following:

- It was discovered that the growth mechanisms depend on the plasma power and the number of passes, as determined by the RMS measurements and SEM and AFM images.
- Two key variables that determine the friction performance of the samples are: [a] the average surface temperature of the samples during the coating process (depending on the plasma power and the number of passes) and [b] the coating thickness. If the average surface temperature exceeds a certain value, the residual thermal stress could compromise the anti-friction ability. However, it is necessary that the substrate surface be covered entirely.

- Successful samples (those with a friction coefficient that is less than the current industrial solutions) were samples that were coated in 6, 12 or 18 passes and a plasma power of 350 W or coated in six passes and a plasma power of 450 W. The average surface temperature of all of these samples during the coating process did not exceed 92 ºC, and the thickness of the coatings was greater than 1000 nm.
- Samples that were coated in six passes and at a power of 350 W proved to have the best friction performance. This sample had a friction coefficient 46% and 53% lower than that of the flocked seals and polyamide tape respectively.
- The wettability of the coated samples depends mainly on the roughness, as no significant chemical variations in the uppermost layer (3 nm) were identified.
- All the studied samples, except the S6/550 sample, had a WCA that was higher than that of the polyamide tape (85.1º ± 7.4) and the uncoated TPE (86.0º ± 6.35). Sample S18/350 had the highest WCA (116.5º ± 7.0). It was 37% higher than the WCA of the polyamide tape.

In future research, the authors will undertake the following:

- Establish the plasma polymerization parameters that provide anti-friction properties that are similar to those of the current industrial solutions, but are less costly. That is, it is not necessary that coatings have friction coefficients as low as discussed in this paper. For instance, the minimum number of passes, with a plasma power of 350 W that is required to obtain a similar friction performance to that of the current industrial solutions will be studied. The intention will be to reduce the costs related to the plasma equipment, plasma gas consumption and other consumables in a future industrial process.

- Finally, in order to standardize this technology in the automotive industry, other tests related to ozone stability, solar radiation, etc., will be implemented.

Acknowledgments

This work was funded by the Regional Research Plan of the Autonomous Community of La Rioja (Spain) through project ADER 2014-I-IDD-00089. The author, E. Sainz-García, thanks the program of pre-doctoral contracts for the training of research staff funded by the University of La Rioja.

Bibliography

[1] F. Alba-Elías, E. Sainz-García, A. González-Marcos, J. Ordieres-Meré, Tribological behavior of plasma-polymerized aminopropyltriethoxysilane films deposited on thermoplastic elastomers substrates, Thin Solid Films. 540 (2013) 125–134. doi:10.1016/j.tsf.2013.06.028.

[2] E. Sainz-García, F. Alba-Elías, R. Múgica-Vidal, M. Pantoja-Ruiz, Promotion of tribological and hydrophobic properties of a coating on TPE substrates by atmospheric plasma-polymerization, Appl. Surf. Sci. 371 (2016) 50–60. doi:10.1016/j.apsusc.2016.02.186.

[3] V. Seitz, K. Arzt, S. Mahnel, C. Rapp, S. Schwaminger, M. Hoffstetter, et al., Improvement of adhesion strength of self-adhesive silicone rubber on thermoplastic substrates - Comparison of an atmospheric pressure plasma jet (APPJ) and a Pyrosil® flame, Int. J. Adhes. Adhes. 66 (2016) 65–72. doi:10.1016/j.ijadhadh.2015.12.009.

[4] N. Ghali, C. Vivien, B. Mutel, A. Rives, Multilayer coating by plasma polymerization of TMDSO deposited on carbon steel : Synthesis and characterization, Surf. Coat. Technol. 259 (2014) 504–516. doi:10.1016/j.surfcoat.2014.10.037.

[5] J. Bardon, K. Apaydin, A. Laachachi, M. Jimenez, T. Fouquet, F. Hilt, et al., Characterization of a plasma polymer coating from an organophosphorus silane deposited at atmospheric pressure for fire-retardant purposes, Prog. Org. Coatings. 88 (2015) 39–47. doi:10.1016/j.porgcoat.2015.06.005.

[6] D. Merche, N. Vandencasteele, F. Reniers, Atmospheric plasmas for thin film deposition: A critical review, Thin Solid Films. 520 (2012) 4219–4236. doi:10.1016/j.tsf.2012.01.026.

[7] E. Mohseni, E. Zalnezhad, A.D. Ahmed, A.R. Bushroa, A study on surface modification of Al7075-T6 alloy against fretting fatigue phenomenon, Surf. Coatings Technol. 2014 (2014) 1–17. doi:10.1016/j.wear.2011.12.005.

[8] N. Kumar, S. a. Barve, S.S. Chopade, R. Kar, N. Chand, S. Dash, et al., Scratch resistance and tribological properties of SiOx incorporated diamond-like carbon films deposited by r.f. plasma assisted chemical vapor deposition, Tribol. Int. 84 (2015) 124–131. doi:10.1016/j.triboint.2014.12.001.

[9] S.M. Hanetho, I. Kaus, A. Bouzga, C. Simon, T. Grande, M.A. Einarsrud, Synthesis and characterization of hybrid aminopropyl silane-based coatings on stainless steel substrates, Surf. Coatings Technol. 238 (2014) 1–8. doi:10.1016/j.surfcoat.2013.10.013.

[10] E. Sainz-García, F. Alba-Elías, R. Múgica-Vidal, A. González-Marcos, Enhanced surface friction coefficient and hydrophobicity of TPE substrates using an APPJ system, Appl. Surf. Sci. 328 (2015) 554–567. doi:10.1016/j.apsusc.2014.12.084.

[11] O. V. Penkov, D.H. Lee, H. Kim, D.E. Kim, Frictional behavior of atmospheric plasma jet deposited carbon-ZnO composite coatings, Compos. Sci. Technol. 77 (2013) 60–66. doi:10.1016/j.compscitech.2013.01.005.

[12] X. Landreau, C. Dublanche-Tixier, C. Jaoul, C. Le Niniven, N. Lory, P. Tristant, Effects of the substrate temperature on the deposition of thin SiOx films by atmospheric pressure microwave plasma torch (TIA), Surf. Coatings Technol. 205 (2011) S335–S341. doi:10.1016/j.surfcoat.2011.03.123.

[13] L. Körner, a. Sonnenfeld, P.R. Von Rohr, Silicon oxide diffusion barrier coatings on polypropylene, Thin Solid Films. 518 (2010) 4840–4846. doi:10.1016/j.tsf.2010.02.006.

[14] E. Kedroňová, L. Zajíčková, D. Hegemann, M. Klíma, M. Michlíček, A.

Manakhov, Plasma enhanced CVD of organosilicon thin films on electrospun polymer nanofibers, Plasma Process. Polym. 12 (2015) 1231–1243. doi:10.1002/ppap.201400235.

[15] M.R. Amirzada, A. Tatzel, V. Viereck, H. Hillmer, Surface roughness analysis of SiO2 for PECVD, PVD and IBD on different substrates, Appl. Nanosci. 6 (2015) 215–222. doi:10.1007/s13204-015-0432-8.

[16] D.S. Wuu, W.C. Lo, C.C. Chiang, H.B. Lin, L.S. Chang, R.H. Horng, et al., Plasma-deposited silicon oxide barrier films on polyethersulfone substrates: temperature and thickness effects, Surf. Coatings Technol. 197 (2005) 253–259. doi:10.1016/j.surfcoat.2004.09.033.

[17] L. Zhou, G.-H. Lv, H. Pang, G.-P. Zhang, S.-Z. Yang, Comparing deposition of organic and inorganic siloxane films by the atmospheric pressure glow discharge, Surf. Coatings Technol. 206 (2012) 2552–2557. doi:10.1016/j.surfcoat.2011.11.011.

[18] B. Verheyde, D. Havermans, A. Vanhulsel, Characterization and tribological behaviour of siloxane-based plasma coatings on HNBR rubber, Plasma Process. Polym. 8 (2011) 755–762. doi:10.1002/ppap.201000136.

[19] L. Marcinauskas, M. Silinskas, A. Grigonis, Influence of standoff distance on the structure and properties of carbon coatings deposited by atmospheric plasma jet, Appl. Surf. Sci. 257 (2011) 2694–2699. doi:10.1016/j.apsusc.2010.10.047.

[20] M. Bedjaoui, B. Despax, Physicochemical and structural properties of ultra thin films with embedded silicon particles, Surf. Coatings Technol. 201 (2007) 9179–9183. doi:10.1016/j.surfcoat.2007.04.006.

[21] L. Korner, Diffusion barrier coatings for polymer containers processed by plasma enhanced chemical vapor deposition, Universität Stuttgart, 2010. http://e-

collection.library.ethz.ch/eserv/eth:1657/eth-1657-02.pdf.

[22] B. Borer, SiOx in a Thin Film Deposition on Particles by Plasma Enhanced Chemical Vapor Deposition Circulating Fluidized Bed Reactor, Swiss Federal Institute of Technology Zurich, 2005. http://e-collection.library.ethz.ch/eserv/eth:28482/eth-28482-02.pdf.

[23] A. Manakhov, M. Moreno-Couranjou, N.D. Boscher, V. Rogé, P. Choquet, J.J. Pireaux, Atmospheric pressure pulsed plasma copolymerisation of maleic anhydride and vinyltrimethoxysilane: influence of electrical parameters on chemistry, morphology and deposition rate of the coatings, Plasma Process. Polym. 9 (2012) 435–445. doi:10.1002/ppap.201100184.

[24] B. Borer, A. Sonnenfeld, P. Rudolf von Rohr, Influence of substrate temperature on morphology of SiOx films deposited on particles by PECVD, Surf. Coatings Technol. 201 (2006) 1757–1762. doi:10.1016/j.surfcoat.2006.03.001.

[25] A. Soum-Glaude, L. Thomas, E. Tomasella, Amorphous silicon carbide coatings grown by low frequency PACVD: structural and mechanical description, Surf. Coatings Technol. 200 (2006) 6425–6429. doi:10.1016/j.surfcoat.2005.11.066.

[26] B. Verheyde, M. Rombouts, A. Vanhulsel, D. Havermans, J. Meneve, M. Wangenheim, Influence of surface treatment of elastomers on their frictional behaviour in sliding contact, Wear. 266 (2009) 468–475. doi:10.1016/j.wear.2008.04.040.

[27] C. Sarra-Bournet, Fonctionnalisation de surface de polymères par plasma à la pression atmosphérique. Amination de surface et dépôt de couches minces par un procédé de décharge par barrière diélectrique, Université Toulouse III - Paul Sabatier, 2009. http://thesesups.ups-tlse.fr/665/1/Sarra-Bournet_Christian.pdf.

[28] S. Bhattacharya, A. Datta, J.M. Berg, S. Gangopadhyay, Studies on surface

wettability of poly(dimethyl) siloxane (PDMS) and glass under oxygen-plasma treatment and correlation with bond strength, J. Microelectromechanical Syst. 14 (2005) 590–597. doi:10.1109/JMEMS.2005.844746.

[29] J. Petersen, J. Bardon, A. Dinia, D. Ruch, N. Gherardi, Organosilicon coatings deposited in atmospheric pressure townsend discharge for gas barrier purpose: Effect of substrate temperature on structure and properties, ACS Appl. Mater. Interfaces. 4 (2012) 5872–5882. doi:10.1021/am3015229.

[30] F. Alba-Elías, J. Ordieres-Meré, A. González-Marcos, Deposition of thin-films on EPDM substrate with a plasma-polymerized coating, Surf. Coatings Technol. 206 (2011) 234–242. doi:10.1016/j.surfcoat.2011.06.054.

[31] M. Touzin, P. Chevallier, F. Lewis, S. Turgeon, S. Holvoet, G. Laroche, et al., Study on the stability of plasma-polymerized fluorocarbon ultra-thin coatings on stainless steel in water, Surf. Coatings Technol. 202 (2008) 4884–4891. doi:10.1016/j.surfcoat.2008.04.088.

[32] C.S. Yang, Y.H. Yu, K.M. Lee, H.J. Lee, C.K. Choi, Investigation of low dielectric carbon-doped silicon oxide films prepared by PECVD using methyltrimethoxysilane precursor, Thin Solid Films. 506–507 (2006) 50–54. doi:10.1016/j.tsf.2005.08.032.

[33] N. Singh, K.K. Reza, M.A. Ali, V.V. Agrawal, A.M. Biradar, Self assembled DC sputtered nanostructured rutile TiO2 platform for bisphenol A detection, Biosens. Bioelectron. 68 (2015) 633–641. doi:10.1016/j.bios.2015.01.041.

[34] N.S.K. Gunda, M. Singh, L. Norman, K. Kaur, S.K. Mitra, Optimization and characterization of biomolecule immobilization on silicon substrates using (3-aminopropyl)triethoxysilane (APTES) and glutaraldehyde linker, Appl. Surf. Sci. 305 (2014) 522–530. doi:10.1016/j.apsusc.2014.03.130.

[35] A. Ramamoorthy, M. Rahman, D. a. Mooney, J.M. Don MacElroy, D.P. Dowling, The Influence of Process Parameters on Chemistry, Roughness and Morphology of Siloxane Films Deposited by an Atmospheric Plasma Jet System, Plasma Process. Polym. 6 (2009) S530–S536. doi:10.1002/ppap.200931109.

[36] E.V. Kober, A.E. Chmel, Recording of IR spectra of polymer specimen surfaces with rough relief using thermoplastic ATR elements, J. Appl. Spectrosc. 64 (1997) 140–145.

[37] R.O. Carter III, M.C. Paputa Peck, D.R. Bauer, The Characterization of Polymer Surfaces by Photoacoustic Fourier Transform Infrared Spectroscopy, Polym. Degrad. Stab. 23 (1989) 121–134.

[38] A. Kondyurin, M. Bilek, Ion Beam Treatment of Polymers, 2008. doi:10.1016/B978-008044692-9.50001-7.

[39] A.J. Choudhury, S.A. Barve, J. Chutia, A.R. Pal, R. Kishore, Jagannath, et al., RF-PACVD of water repellent and protective HMDSO coatings on bell metal surfaces: Correlation between discharge parameters and film properties, Appl. Surf. Sci. 257 (2011) 8469–8477. doi:10.1016/j.apsusc.2011.04.134.

[40] F. Fanelli, A.M. Mastrangelo, F. Fracassi, Aerosol-assisted atmospheric cold plasma deposition and characterization of superhydrophobic organic-inorganic nanocomposite thin films, Langmuir. 30 (2014) 857–865. doi:10.1021/la404755n.

[41] H. Hamze, M. Jimenez, D. Deresmes, A. Beaurain, N. Nuns, M. Traisnel, Influence of processing gases on the properties of cold atmospheric plasma SiOxCy coatings, Appl. Surf. Sci. 315 (2014) 531–537. doi:10.1016/j.apsusc.2013.12.108.

[42] D.J. Marchand, Z.R. Dilworth, R.J. Stauffer, E. Hsiao, J.-H. Kim, J.-G. Kang, et

al., Atmospheric rf plasma deposition of superhydrophobic coatings using tetramethylsilane precursor, Surf. Coatings Technol. 234 (2013) 14–20. doi:10.1016/j.surfcoat.2013.03.029.

[43] S. Podgoric, B.J. Jones, R. Bulpett, G. Troisi, J. Franks, Diamond-like carbon/epoxy low-friction coatings to replace electroplated chromium, Wear. 267 (2009) 996–1001. doi:10.1016/j.wear.2009.01.014.

[44] G. Montay, A. Cherouat, A. Nussair, J. Lu, Residual stresses in coating technology, J. Mater. Sci. 20 (2004) 81–84.

[45] A. Kariminejad, E. Taheri-Nassaj, M. Ghanbarian, S.A. Hassanzadeh-Tabrizi, Effects of PACVD parameters including pulsed direct current and deposition time on nanostructured carbon coating deposited on carbon fiber fabrics, Mater. Des. 106 (2016) 184–194. doi:10.1016/j.matdes.2016.05.072.

[46] A.E.A. Zeghni, The effect of thin film coatings and nitriding on the mechanical properties and wear resistance of tool steel, Dublin City University, 2003.

List of tables

List of figures

Fig. 16. Evolution of the friction coefficient of: samples coated at 350 W (S2/350, S6/350, S12/350, S18/350) and 550 W (S2/550, S6/550, S12/550, S18/550), uncoated TPE, flocked seal and polyamide tape.

Fig. 17. Average friction coefficient of the coated samples, the uncoated TPE, flocked seal and the polyamide tape.

Fig. 18. SEM (top) and EDX (bottom) images with a magnification of x300 of the wear track of sample S18/550 after a 4000 m friction test: [a] and [c] limited area coating-wear track, [b] and [d] central area of the wear track. The dashed arrows indicate the sliding direction and the white circles indicate coating debris.

Table 1

Sample	Power (W) (activation and polymerization)	Number of passes (activation)	Number of passes (polymerization)	Deposition time (s) (polymerization)	Average Surface Temperature (ºC)
A1/350	350W	1	-	-	68.3
S2/350		1	2	75	70.0
S6/350		1	6	224	75.3
S12/350		1	12	449	79.5
S18/350		1	18	673	82.4
A1/450	450W	1	-	-	81.7
S2/450		1	2	75	83.8
S6/450		1	6	224	90.5
S12/450		1	12	449	94.6
S18/450		1	18	673	97.6
A1/550	550W	1	-	-	98.0
S2/550		1	2	75	101.1
S6/550		1	6	224	108.0
S12/550		1	12	449	113.1
S18/550		1	18	673	116.3

Table 1. Sample identification and deposition conditions of each sample.

Table 2

Sample	Thickness (nm)	Standard deviation (SD)	Roughness (nm)	Standard deviation (SD)
A1/350	-	-	405	13
S2/350	230	47	401	31
S6/350	1524	559	338	45
S12/350	2123	503	461	37
S18/350	2938	854	724	48
A1/450	-	-	406	22
S2/450	190	19	276	22
S6/450	1483	413	257	25
S12/450	2563	448	413	35
S18/450	2871	754	636	51
A1/550	-	-	389	19
S2/550	160	32	376	28
S6/550	1402	407	322	30
S12/550	2475	398	376	29
S18/550	2880	863	629	49
Uncoated TPE	-	-	364	32

Table 2. Thickness and roughness of all the analyzed samples.

Table 3

Sample	Atomic chemical composition (at. %)			
	C1s	**O1s**	**Si2p**	**N1s**
A1/350	81.0	15.2	3.0	0.8
S2/350	64.2	20.7	11.7	3.4
S6/350	55.3	26.5	14.1	4.2
S12/350	58.0	24.9	13.7	3.4
S18/350	56.7	25.2	14.1	4.1
A1/450	82.5	14.4	1.7	1.4
S2/450	60.9	23.6	12.0	3.5
S6/450	58.3	24.8	13.3	3.7
S12/450	58.2	24.8	13.6	3.4
S18/450	53.1	28.1	14.8	4.0
A1/550	93.0	6.2	0.7	0.1
S2/550	58.4	24.1	14.4	3.2
S6/550	54.0	27.6	15.1	3.3
S12/550	58.3	25.0	13.4	3.4
S18/550	51.4	28.7	16.6	3.3
Uncoated TPE	94.3	4.5	1.2	-

Table 3. Atomic chemical composition (at. %) of all the analyzed samples.

Table 4

Sample	Relative percentage (%)		
	SiO_2 (~102.1 eV)	**SiO_3 (~102.8 eV)**	**SiO_4 (~103.4 eV)**
S2/350	-	7.9	3.8
S2/550	-	7.4	7.0
S6/350	2.0	5.0	7.0
S6/550	0.0	5.2	10.0
S12/350	2.0	6.2	5.5
S12/550	1.8	5.8	7.6
S18/350	3.6	3.9	6.6
S18/550	0.0	7.3	9.3

Table 4. Relative percentage (%) of SiO_2, SiO_3 and SiO_4 of samples coated at 350W and 550W.

Table 5

Sample	Average friction coefficient
S2/350	0.43 ± 0.03
S6/350	0.13 ± 0.02
S12/350	0.14 ± 0.01
S18/350	0.17 ± 0.01
S2/450	0.39 ± 0.04
S6/450	0.24 ± 0.02
S12/450	0.25 ± 0.10
S18/450	0.35 ± 0.19
S2/550	0.39 ± 0.02
S6/550	0.41 ± 0.20
S12/550	0.44 ± 0.05
S18/550	0.36 ± 0.06
Uncoated TPE	0.68 ± 0.02
Flocked seal	0.25 ± 0.06
Polyamide tape	0.28 ± 0.01

Table 5. Average friction coefficient of all of the coated samples, the uncoated TPE, flocked seal and the polyamide tape.

Figure 1

Click here to download high resolution image

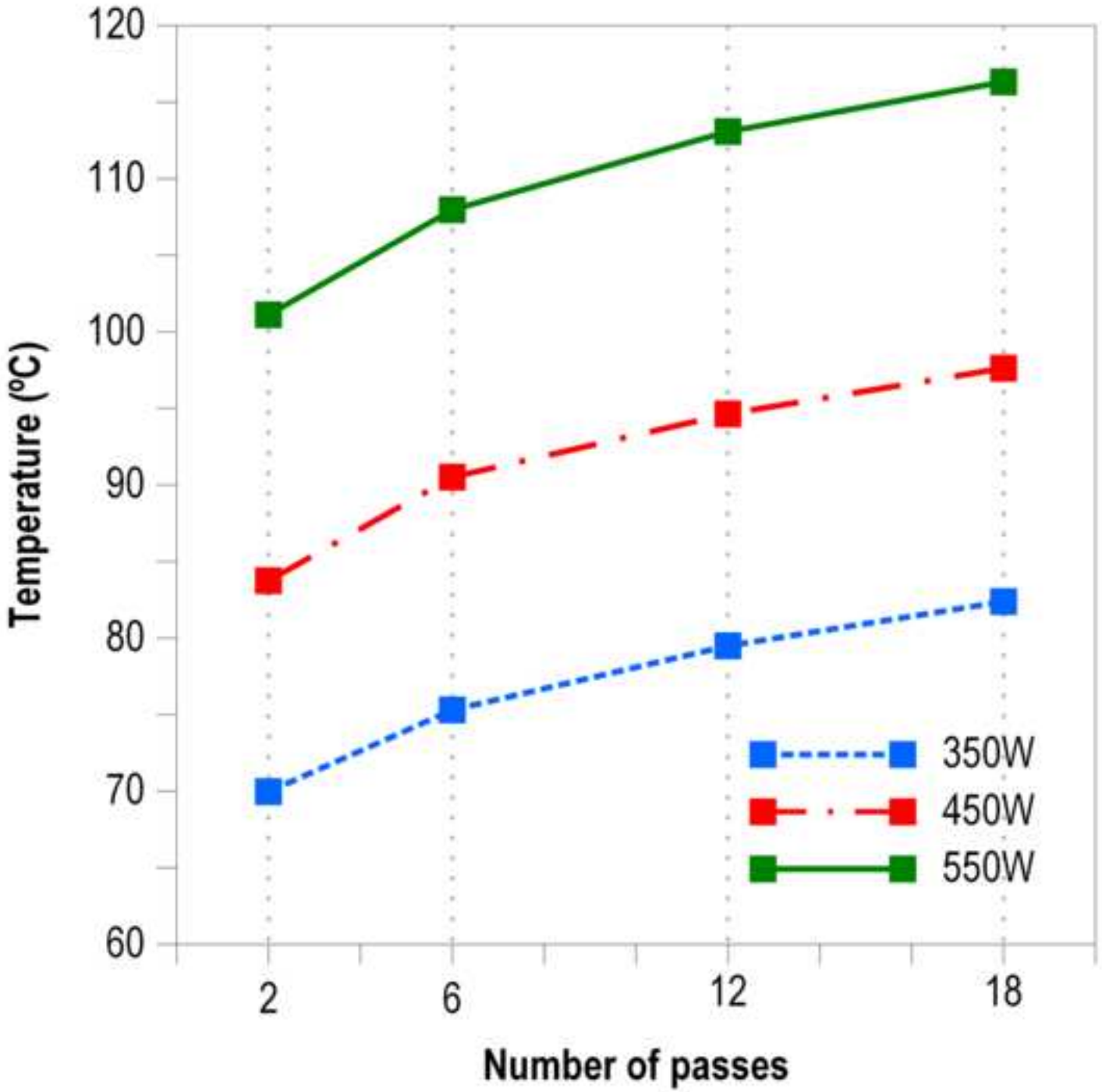

Figure 2

Click here to download high resolution image

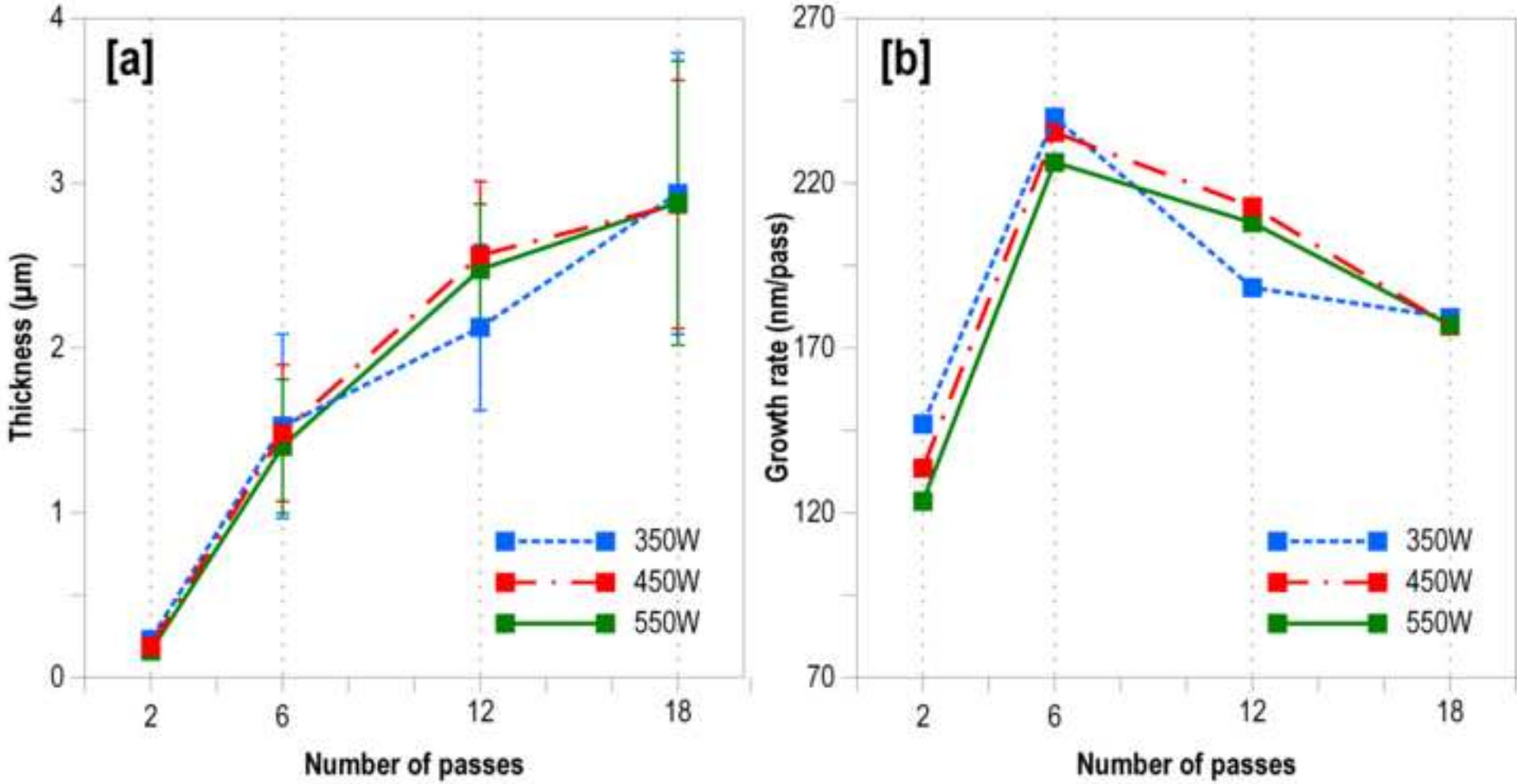

Figure 3

Click here to download high resolution image

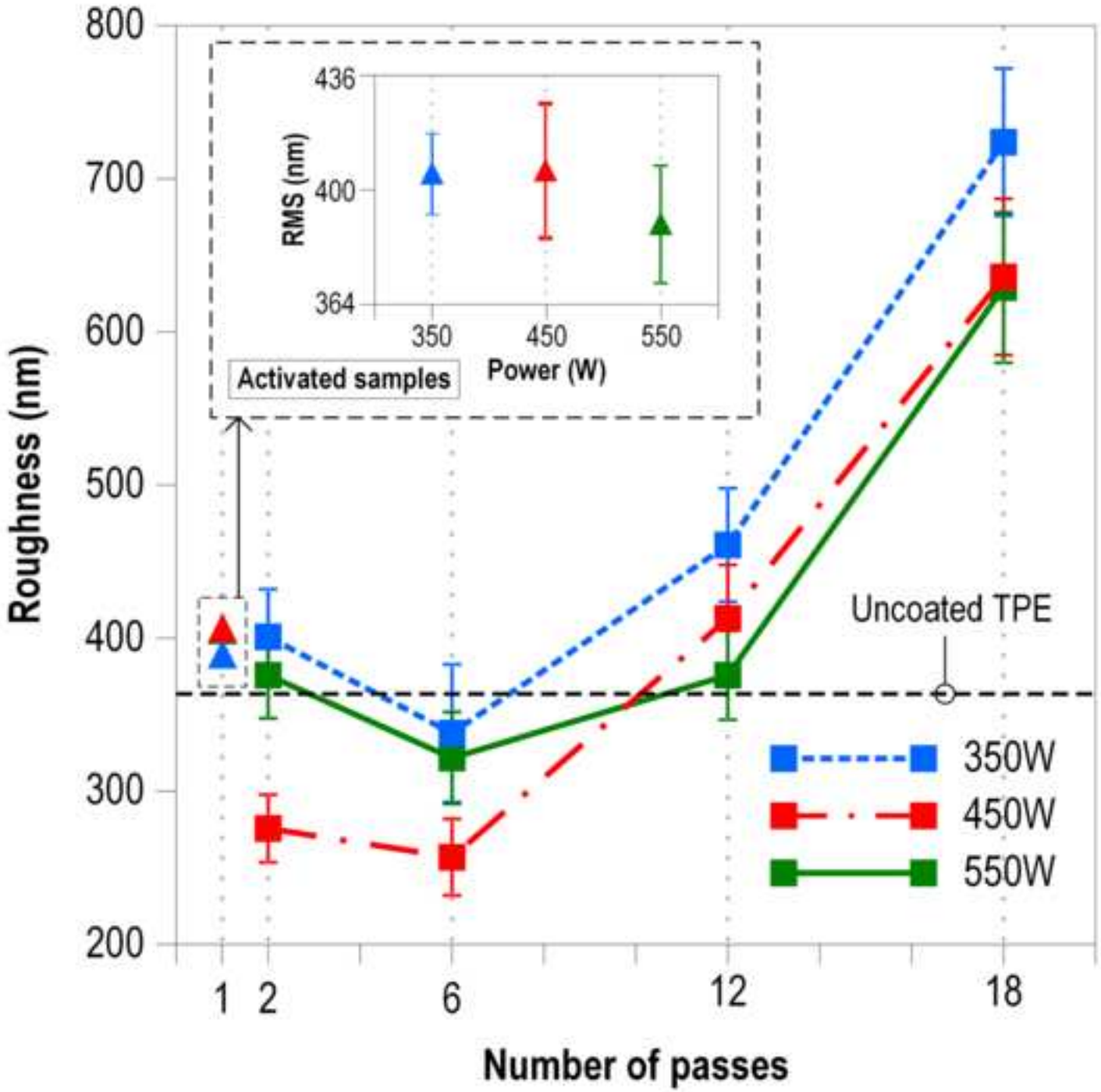

Figure 4

Click here to download high resolution image

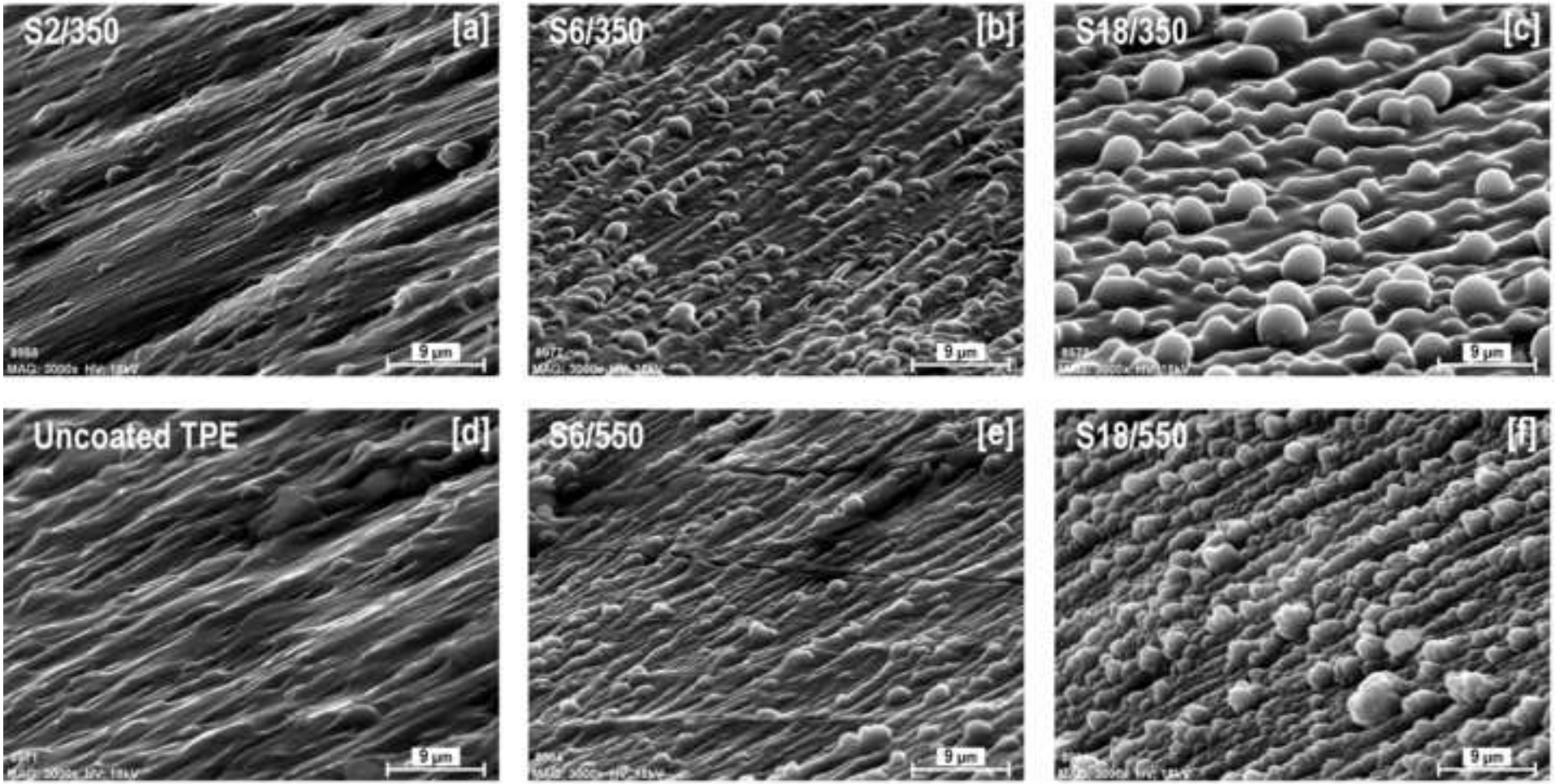

Figure 5

Click here to download high resolution image

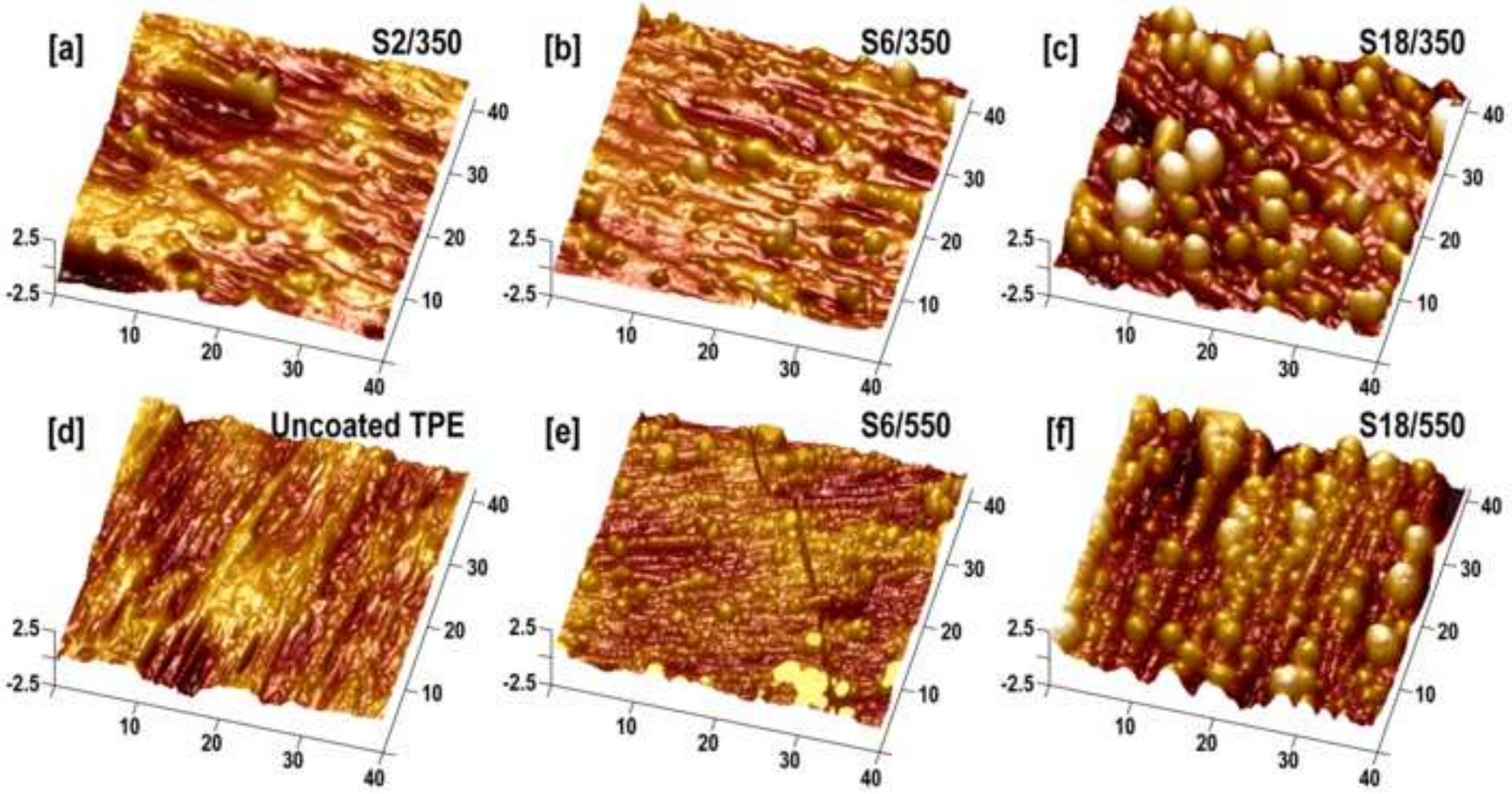

Figure 6

Click here to download high resolution image

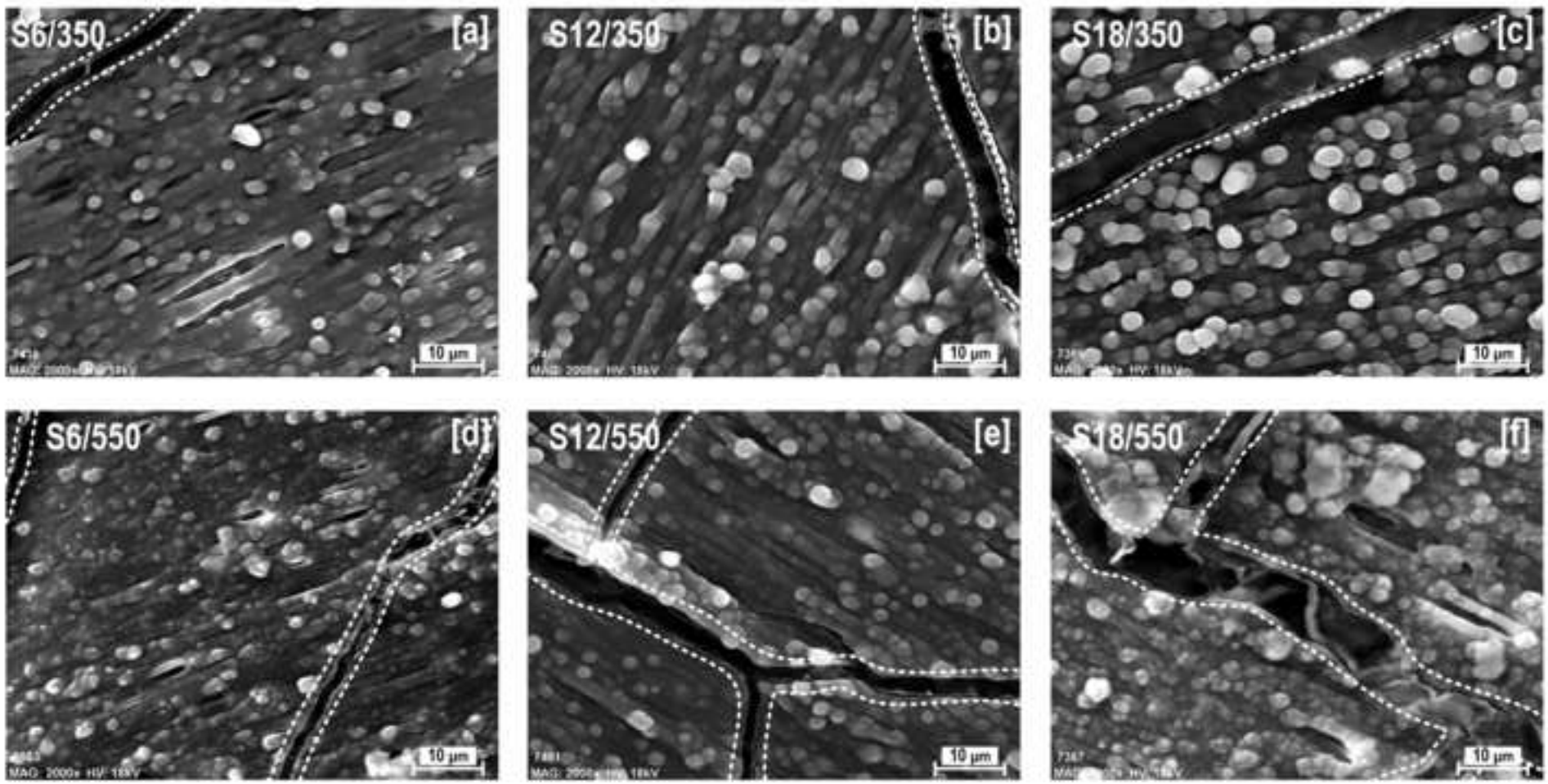

Figure 7

Click here to download high resolution image

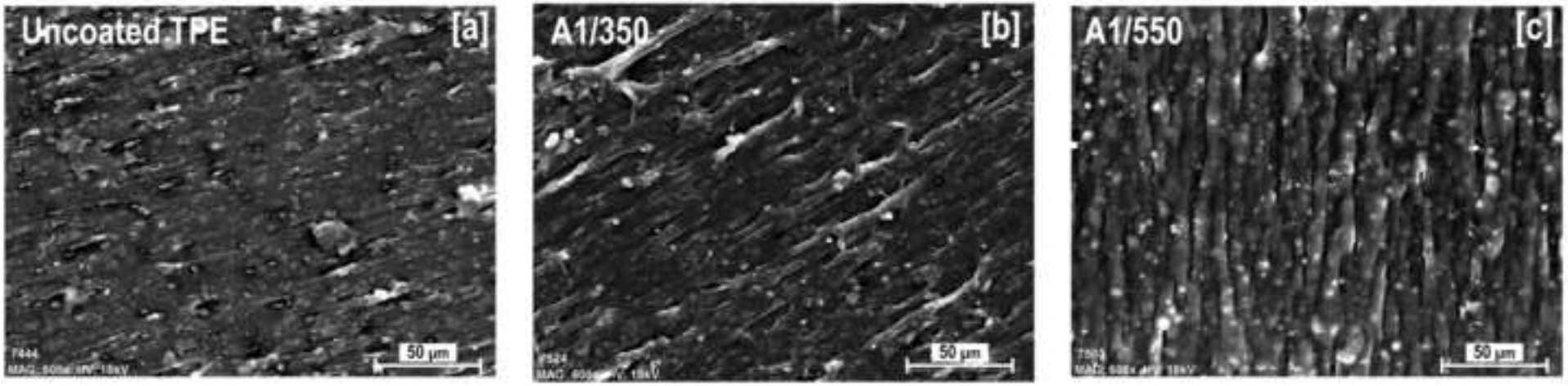

Figure 8

Click here to download high resolution image

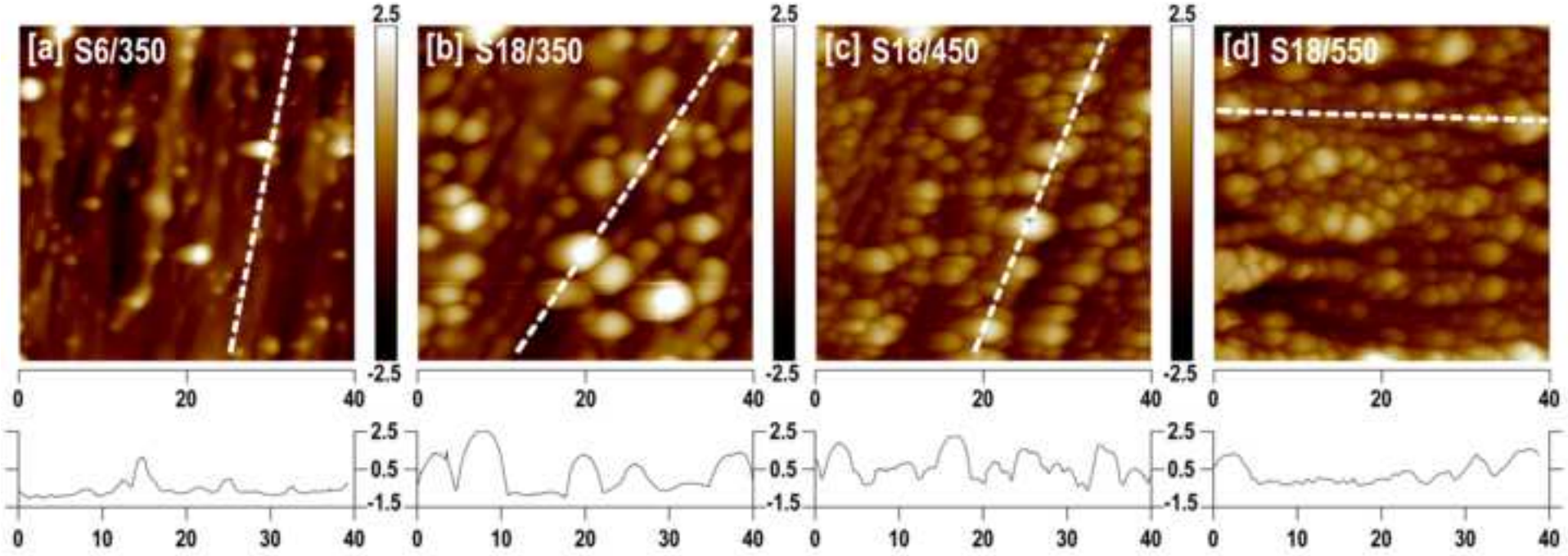

Figure 9

Click here to download high resolution image

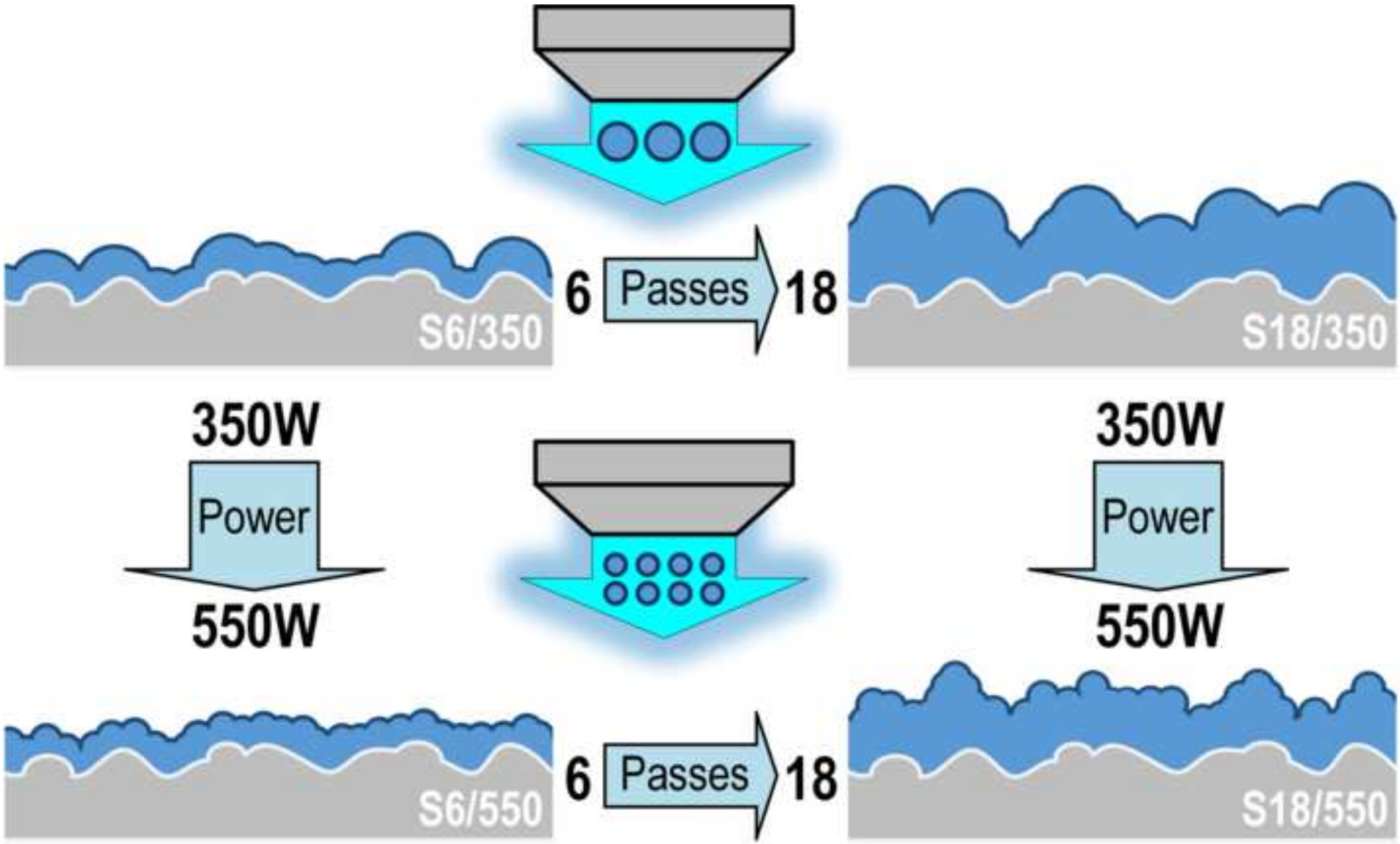

Figure 10

Click here to download high resolution image

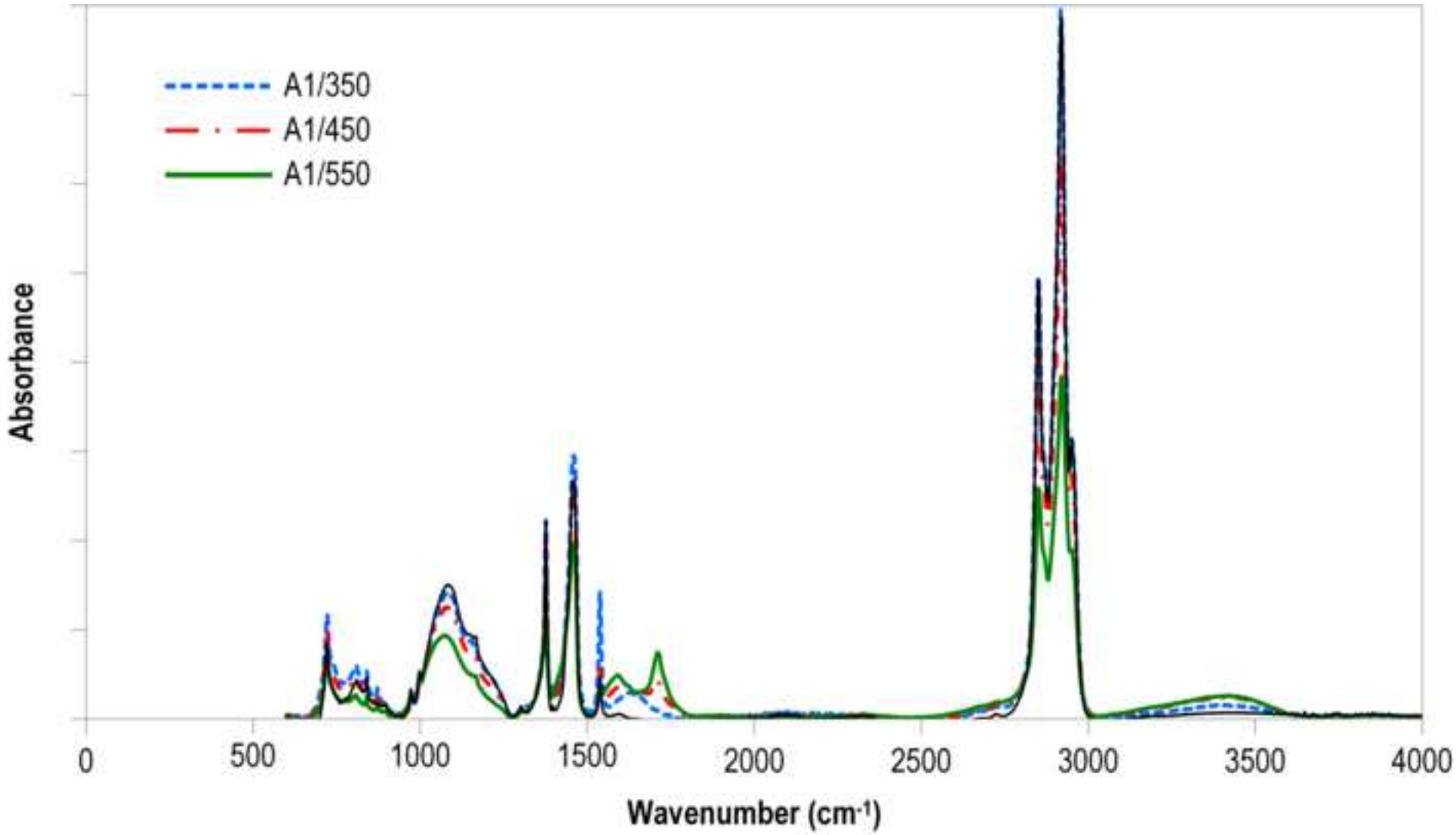

Figure 11
Click here to download high resolution image

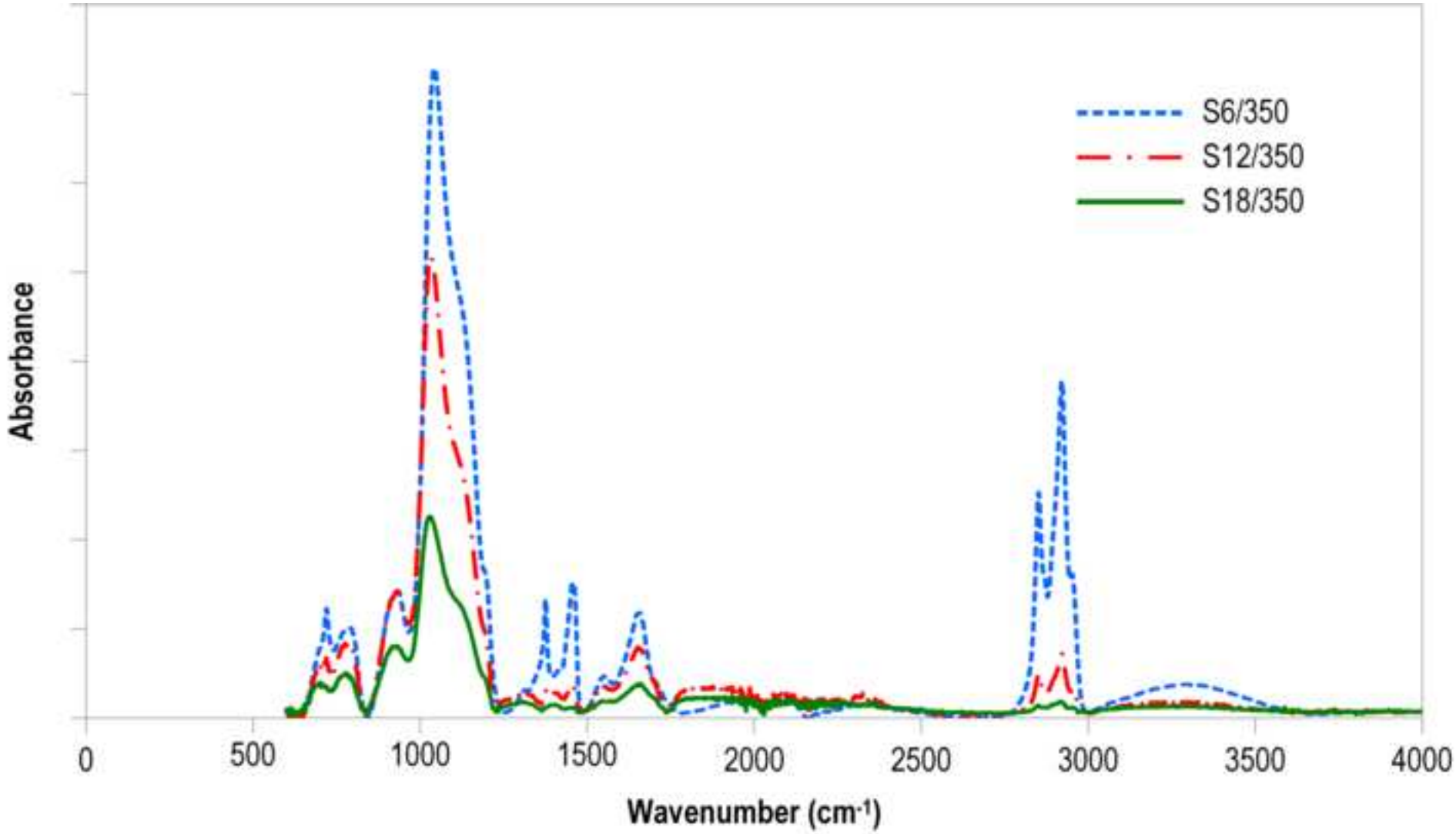

Figure 12

Click here to download high resolution image

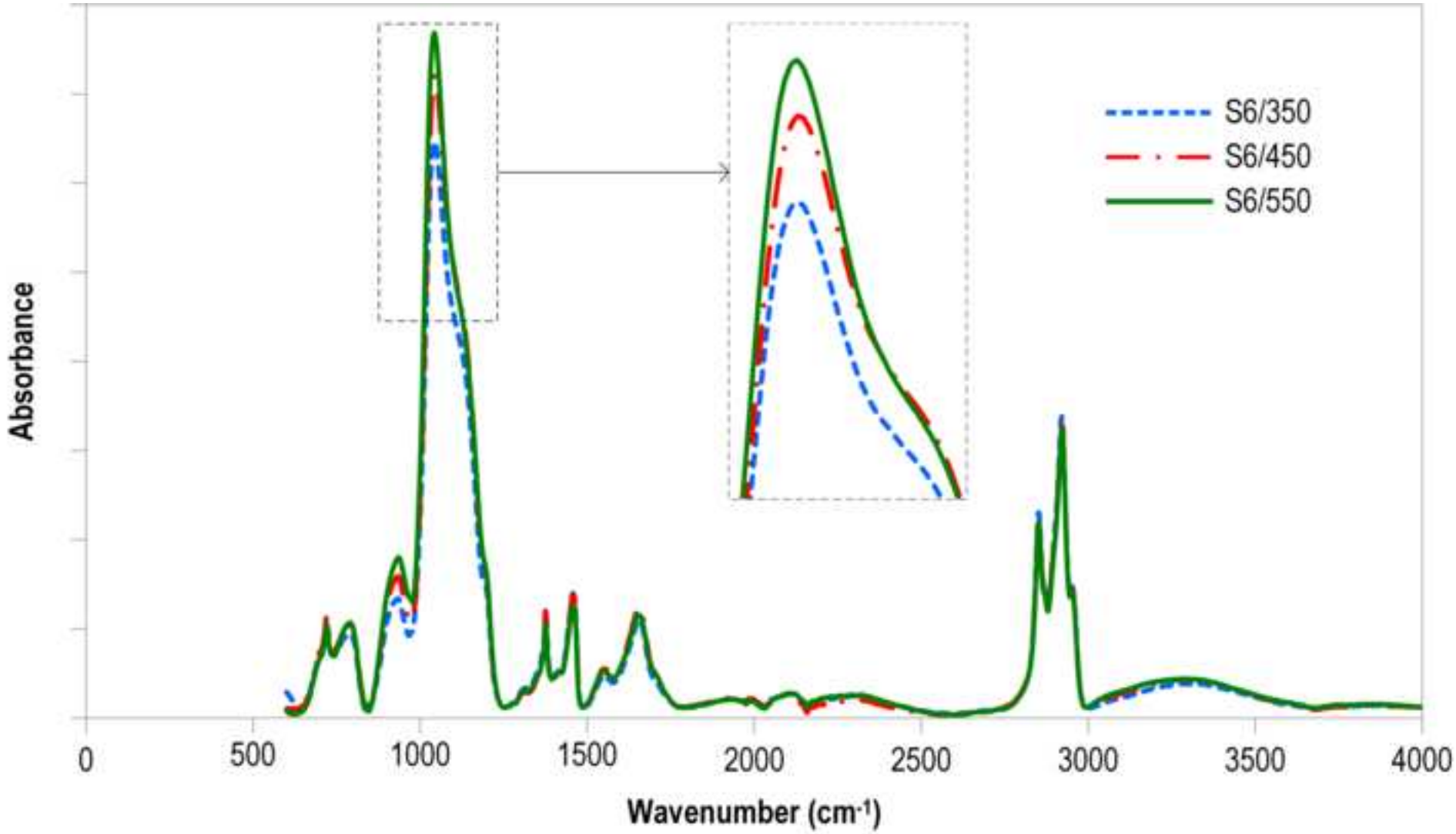

Figure 13

Click here to download high resolution image

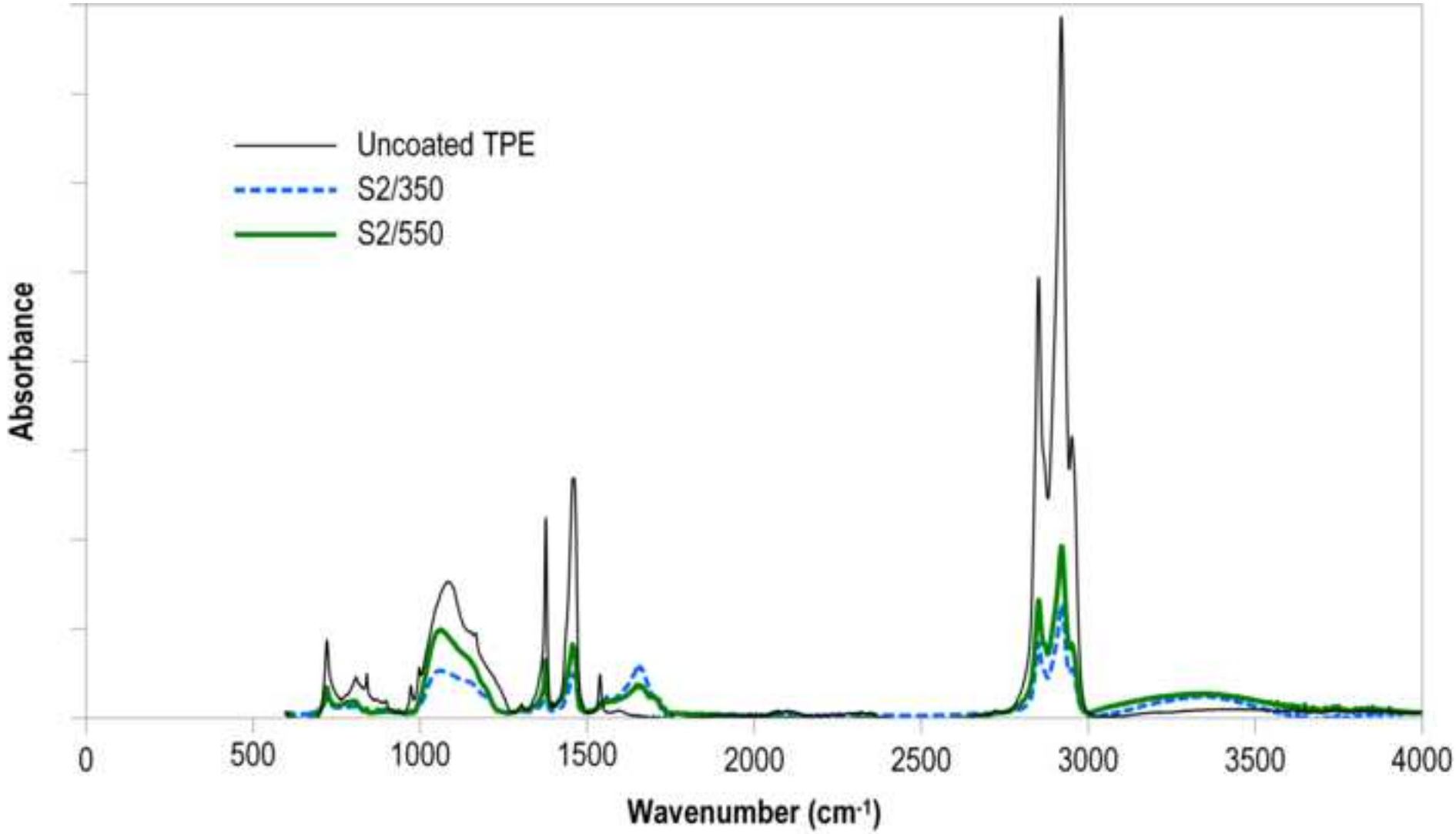

Figure 14

Click here to download high resolution image

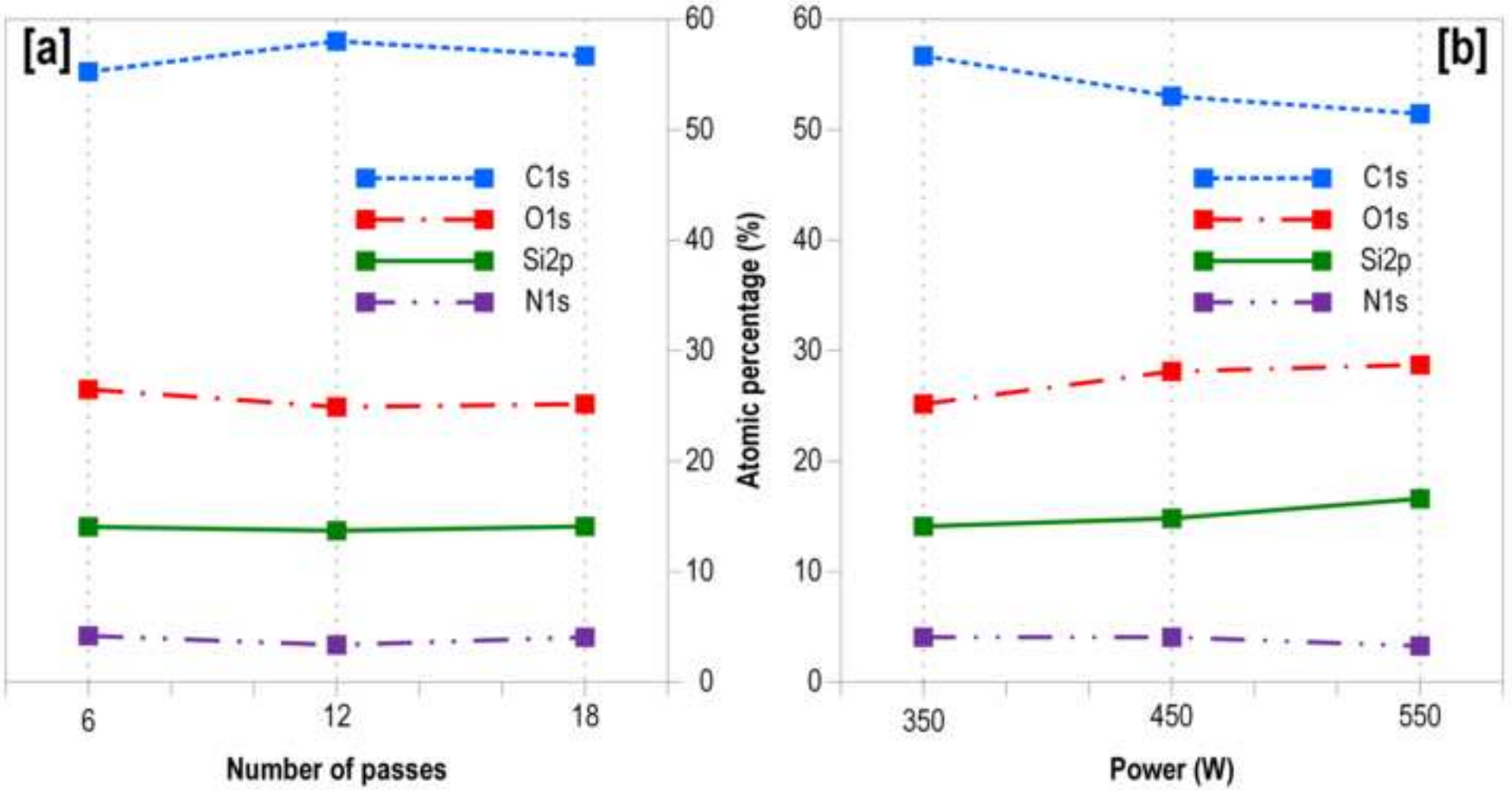

Figure 15

Click here to download high resolution image

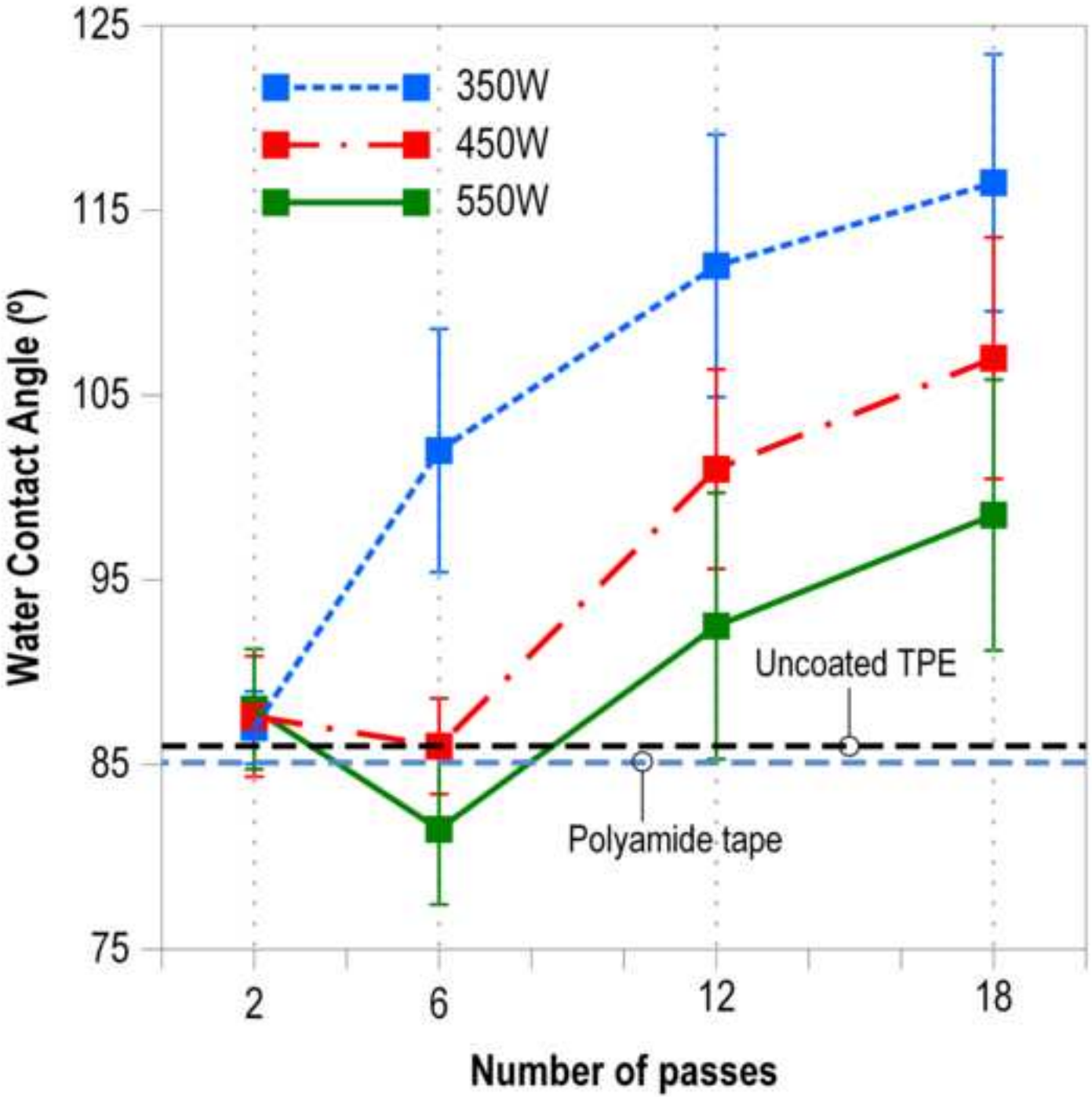

Figure 16

Click here to download high resolution image

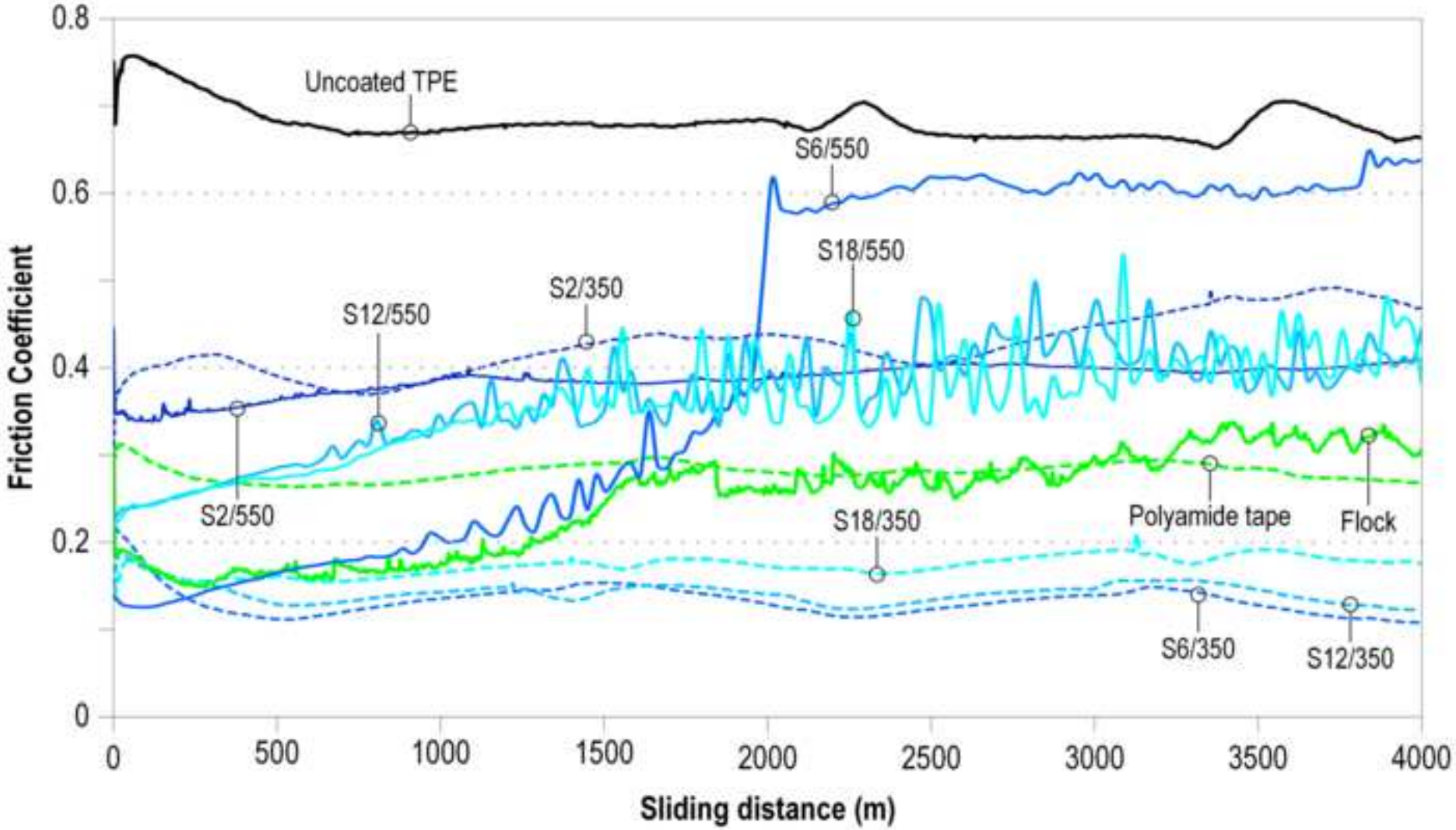

Figure 17

Click here to download high resolution image

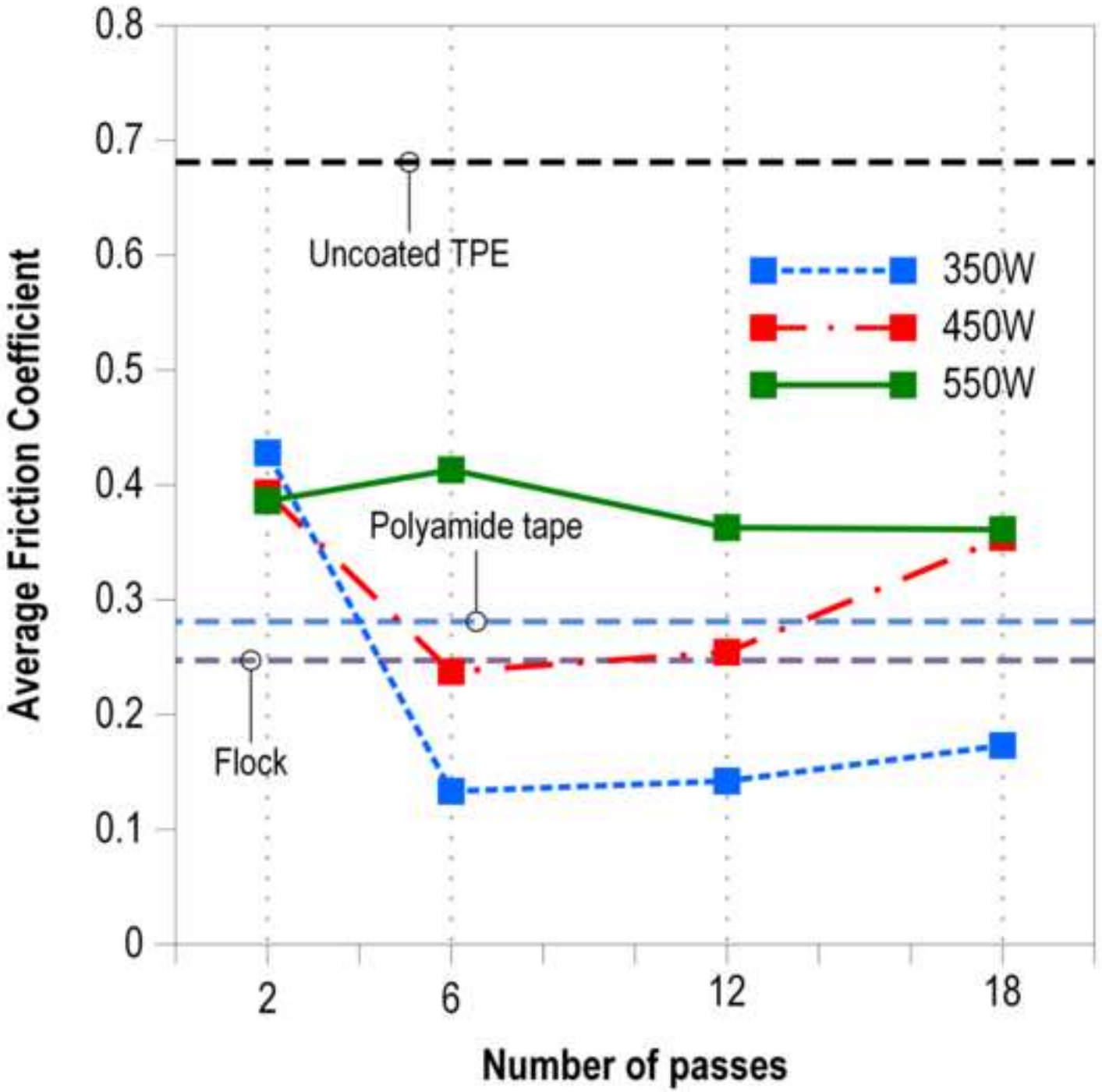

Figure 18

Click here to download high resolution image

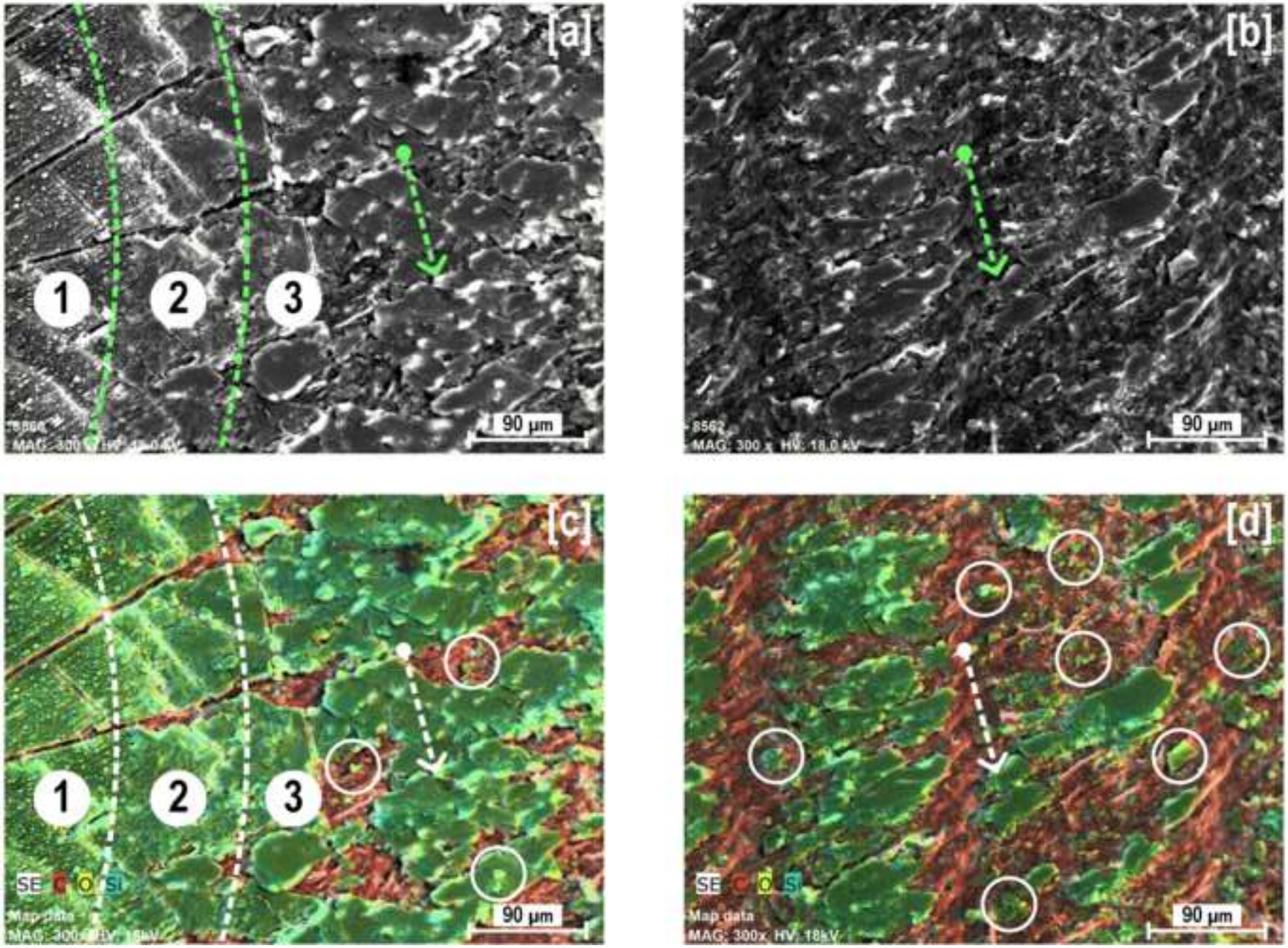

Graphical Abstract

Click here to download high resolution image